Supporting Information

Squalene Based Nanocomposites: A New Platform for the Design of Multifunctional Pharmaceutical Theragnostics

José L. Arias[1°], L. Harivardhan Reddy[2°#], Mohammad Othman[2°], Brigitte Gillet[3], Didier Desmaële[2], Fatima Zouhiri[2], Franco Dosio[4], Ruxandra Gref[2], Patrick Couvreur[2,]*

[1]Departamento de Farmacia y Tecnología Farmacéutica, Facultad de Farmacia, Universidad de Granada, 18071 – Granada, Spain. Phone: (+34) 958 24 39 02. Fax: (+34) 958 24 89 58. E-mail: jlarias@ugr.es

[2,*]Université Paris-Sud XI, Faculté de Pharmacie, UMR CNRS 8612, IFR 141, 92296 Châtenay-Malabry Cedex, France. Phone: (+33) 1 46 83 53 96. Fax: (+33) 1 46 61 93 34. E-mail: harivardhanr@gmail.com, mohammad.othman@u-psud.fr, didier.desmaele@u-psud.fr, fatima.zouhiri@u-psud.fr, ruxandra.gref@u-psud.fr, patrick.couvreur@u-psud.fr

[#]Current address: Sanofi-aventis, 13 Quai Jules-Guesdes 94403 Vitry-sur-Seine France.

[3]Université Paris-Sud XI, UMR CNRS 8081, 91405 Orsay Cedex, France; and, Laboratoire de Résonance Magnétique Nucléaire Biologique-Institut de Chimie des Substances Naturelles, Gif sur Yvette, France. Phone: (+33) 1 69 15 41 35. Fax: (+33) 1 69 15 41 36. E-mail: brigitte.gillet@u-psud.fr

[4]Università degli Studi di Torino, Facoltà di Farmacia, Dipartimento di Scienza e Tecnologia del Farmaco, 10125 Torino, Italy. Phone: (+39) 0116707697. Fax: (+39) 0112367697. E-mail: franco.dosio@unito.it

°have equally participated to the present publication

TABLE OF CONTENTS

EXPERIMENTAL SECTION

1. Materials

All the chemicals used were of analytical grade and were used without further purification. Gemcitabine hydrochloride was purchased from Sequoia Research Products Ltd. (Oxford, UK), paclitaxel was from Indena (Milan, Italy), daunorubicin was from APAC Pharmaceutical (Zhejiang, China). cis-Diamminedichloroplatinum (II), pluronic® F-68, squalene, formamide, dextrose, ethyl chloroformate, 1-ethyl-3-(3-dimethylaminopropyl) carbodiimide hydrochloride (EDCI·HCl), pyridine, gadolinium (III) chloride hexahydrate, bromoacetic acid, ammonium bicarbonate xylenol orange sodium salt indicator for metal titration, and pyrene were purchased from Sigma-Aldrich Chemical Co. (Paris, France). Chelex 100 sodium form Chelating Resin, and AG1-X4® Resin were from Bio-Rad Laboratories. Sodium azide, *tert*-butanol and Amberlite® IR 120 H resin were from Acros Organics (Geel, Belgium). Lithium hydroxide-monohydrate was purchased from Merck (Germany), potassium carbonate was from Carlo Erba (Milan, Italy). 1,4,7,10-tetraazacyclododecane-1,4,7-triacetic acid triethyl ester (DO3AEt) was purchased from Chematek (Le Pontet, France). Dialysis membranes Spectra/Por® cellulose ester (CE) (molecular weight cut-off (MWco) = 500 Da) was

purchased from Spectrum Laboratories, Inc. (CA, USA). Phosphate buffered saline (PBS, pH = 7.4 ± 0.1) was purchased from BioWhittaker® DPBS (Lonza, Belgium). All other chemicals were from Prolabo (Fontenay-sous-Bois, France). Water used for the experiments was deionized and filtered through membrane filter (Milli-Q Academic, Millipore, France).

2. Methods

2.1. General

All these reactions were performed under nitrogen atmosphere unless stated otherwise. Pyridine, triethylamine, toluene, acetonitrile, dichloromethane, and *N,N*-dimethylformamide (DMF) were distilled over calcium hydride, and stored over 4 Å molecular sieves. Ethyl ether and tetrahydrofuran (THF) were distilled from sodium benzophenone ketyl. Analytical thin-layer chromatography was performed on silica gel $60F_{254}$ glass precoated plates (0.25 mm layer) or RP-18 (F_{254}) plates (Merck, Germany). TLC plates were viewed under UV light (254 nm) and visualized with I_2, Kägi-Misher or Draggendorf reagents. Column chromatography was performed on silica gel 60 (230-400 mesh ASTM) (Merck, Germany). A C-18 reversed-phase 100 silica gel was used for column chromatography of the Gd^{3+} complex (particle size 40-63 µm, surface coverage 17-18 %) (Fluka, Switzerland). High resolution transmission electron microscopy (HRTEM) photographs were obtained using a STEM PHILIPS CM20 (The Netherlands) high resolution transmission microscope set at 80 kV accelerating voltage. The ^{1}H and ^{13}C NMR spectra were recorded on Bruker Avance 300 (300 MHz and 75 MHz, for ^{1}H and ^{13}C, respectively) or Bruker Avance 400 (400 MHz and 100 MHz, for ^{1}H and ^{13}C,

respectively) spectrometers (USA). Shifts of ^{1}H and ^{13}C NMR spectra were calibrated against the solvent residual peak. Recognition of methyl, methylene, methine, and quaternary carbon nuclei in ^{13}C NMR spectra rests on the *J*-modulated spin-echo sequence. Infrared (IR) spectra were obtained as solid or neat liquid on a Fourier Transform Bruker Vector 22 spectrometer (USA). Only significant absorption bands are listed. Low resolution mass spectra (MS) were recorded using electrospray ionization (ESI) conditions in a positive-ion or a negative-ion mode on an Esquire LC Bruker spectrometer (USA). High-resolution mass spectra (HRMS) were recorded using either ESI or MALDI-TOF ionization on a LCT mass spectrometer (Waters, USA) or a Voyager-DE STR mass spectrometer (Applied Biosystems; USA). Elemental analyses were performed with a Perkin Elmer 2400 analyzer (USA) (Service de microanalyse, Centre d'Etudes Pharmaceutiques, Châtenay-Malabry, France). The gadolinium content in the complex was determined at the Service Central d'Analyse du CNRS (Solaize, France) by Inductively Coupled Plasma Atomic Emission Spectroscopy (ICP-AES) with an ICP-AES - JOBIN YVON spectrometer (China).

2.2. Synthesis of nanomagnetite (USPIO)

Nanomagnetite (USPIO) (Figure S1; average diameter and polydispersity index: 9 ± 2 nm and 0.132, respectively) was prepared following the chemical co-precipitation method proposed by Massart.[1] Briefly, 40 mL of an aqueous solution of 1 mol/L $FeCl_3$ (at a rate of 4 mL/min), and 10 mL of an aqueous solution of 2 mol/L $FeCl_2$ in 2 mol/L HCl (at a rate of 1 mL/min) were mixed (at 25.0 ± 0.5 °C, under mechanical stirring: 700 rpm) to 500 mL of a 0.7 mol/L aqueous ammonia solution. In order to obtain stable acidic sols,

the USPIO nanoparticles (NPs) produced were magnetically decanted and redispersed in a 2 mol/L perchloric acid solution. After 12 h, the magnetic colloid was then subjected to a cleaning procedure that included repeated cycles of centrifugation (40 min at 40000 rpm, Centrikon T-124 high-speed centrifuge, Kontron, France) and re-dispersion in water, until the conductivity of the supernatant was ≤ 10 μS/cm. For characterization purposes, the particles were dried at 60.0 ± 0.5 °C in a vacuum oven and stored until their use.

2.3. Synthesis of 4-(N)-trisnorsqualenoyl gemcitabine (SQgem)

4-(*N*)-trisnorsqualenoyl gemcitabine (SQgem) was prepared by covalent coupling of gemcitabine with 1,1',2-trisnorsqualenic acid (**1**) onto the amino group of the nucleoside heterocycle (Figure S2a).[2] To an ice-cooled solution of 1,1',2-trisnorsqualenoic acid (**1**) (0.5 g, 1.2 mmol) and triethylamine (0.15 g, 1.4 mmol) in anhydrous THF (3 mL) was added dropwise a solution of ethyl chloroformate (0.135 g, 1.2 mmol) in anhydrous THF (3 mL). The mixture was stirred at 0 °C for 15 min and a solution of gemcitabine hydrochloride (0.37 g, 1.2 mmol) and triethylamine (0.15 g, 1.4 mmol) in anhydrous DMF (5 mL) was added dropwise to the reaction mixture at the same temperature. The reaction mixture was stirred for 72 h at 25.0 ± 0.5 °C, and then concentrated in vacuum. Aqueous sodium hydrogen carbonate was added, and the mixture was extracted with ethyl acetate. The combined extracts were washed with water, dried over $MgSO_4$, and concentrated under reduced pressure. The crude product was purified by chromatography on silica gel eluting with 1 to 5 % methanol in dichloromethane to give pure SQgem (**3**) as an amorphous white solid (0.46 g, 57 %).

$[\alpha]_D$ = 3.1 (c = 0.95, CH_2Cl_2); IR (neat, cm^{-1}) 3500-3150, 2950, 2921, 2856, 1709, 1656, 1635, 1557, 1490, 1435, 1384, 1319, 1275, 1197, 1130, 1071; ^{1}H NMR (300 MHz, $CDCl_3$) δ: 9.15 (broad s, 1 H, NHCO), 8.16 (d, 1 H, *J* = 7.5 Hz, H6), 7.47 (d, 1 H, *J* = 7.5 Hz, H5), 6.18 (t, 1 H, *J* = 7.0 Hz, H1'), 5.22-5.15 (m, 5 H, *H*C=C(CH_3)), 4.49 (m, 1 H, H3'), 4.86-4.09 (m, 3 H, H4' and H5'), 2.55 (m, 2 H), 2.38-2.28 (m, 2 H), 2.13-1.91 (m, 16 H, C*H*$_2$), 1.69-1.55 (m, 18 H, C=C(C*H*$_3$)); ^{13}C NMR (75 MHz, $CDCl_3$) δ: 173.7 (*C*ONH), 163.0 (HN*C*=N), 155.8 (N*C*ON), 145.4 (CH, C6), 135.1 (C), 134.9 (2 C), 132.7 (C), 131.2 (C), 125.7 (CH), 124.4 (2 CH), 124.2 (2 CH), 122.4 (CF_2), 97.7 (CH, C5), 81.7 (2 CH), 69.2 (CH), 59.9 (CH_2), 39.7 (2 CH_2), 39.5 (CH_2), 36.5 (CH_2), 34.3 (CH_2), 28.3 (2 CH_2), 26.8 (CH_2), 26.7 (CH_2), 26.6 (CH_2), 25.6 (CH_3), 17.6 (CH_3), 16.0 (3 CH_3), 15.8 (CH_3); MS (CI, isobutane): *m/z* (%): 646 (100 %); Anal. Calcd for $C_{36}H_{53}N_3O_5$: C, 66.95, H, 8.27, N, 6.51. Found: C, 66.76, H, 8.40, N, 6.39.

2.4. Synthesis of 14-trisnorsqualenoyl doxorubicin ester (SQdox)

14-*tris*norsqualenoyl-doxorubicin ester (SQdox) (**6**) was prepared by nucleophilic substitution reaction of the 14-bromo-daunorubicin with 1,1',2-trisnorsqualenic acid potassium salt (Figure S2b). Trimethylorthoformate (0.20 mL, 1.83 mmol) was added to a solution of daunorubicin hydrochloride (0.20 g, 0.35 mmol) dissolved in methanol/1,4-dioxane (v/v 1:2, 12 mL). The reaction mixture was stirred at room temperature for 20 min. To the mixture was added a $Br_2/CHCl_3$ (w/v 1:9, 0.68 mL, 0.43 mmol) solution, and the mixture was then stirred for 40 min at 30.0 ± 0.5 °C. The resulting mixture was poured into dry ether (200 mL), the solid residue was filtered and washed with ether (3 x 50 mL). The solid was recrystallized from

acetone/ether (v/v 1:1, 10 mL) and dried to give 14-bromo-daunorubicin (**5**) (0.185 g, 82 %) as a red solid: m.p. 175–176 °C.

The 14-bromo-daunorubicin hydrochloride (**5**) (0.3 g, 0.47 mmol), dissolved in dry acetone (200 mL) was reacted with squalene acid (**1**) (0.376 g, 0.94 mmol) in the presence of potassium carbonate (0.195 g, 1.41 mmol). After 20 h at room temperature the reaction was filtered, the solvent was evaporated and the crude product was purified on silica gel eluting with 10 to 25 % methanol in dichloromethane to give pure SQdox as an amorphous red solid (0.31 g, 71 %). The SQdox was converted to its hydrochloride salt by adding a titrated solution of HCl in ether to a THF solution of the compound and then stirring at -20.0 ± 0.5 °C for 2 h. ^{1}H NMR ($CDCl_3$) δ: 8.02 (d, 1H, H-3), 7.87 (d, 1H, H-1), 7.70 (t, 1H, H-2), 5.46 (s, 1H, H-10), 5.3-5.25 (m, 2H, H-14a, H-14b) and 5.20 (s, 5H, C(sq-H) 5.19 (s, 1H, H-7), 4.15 (q, 1H, H-50), 4.01 (s, 3H, OCH_3), 3.74 (m, 2H, H-30, H-40), 3.24 (d, 1H, H-10), 3.00 (d, 1H, H-10), 2.43 (m, 1H, H-8), 2.29 and 2.35 (s 4H, CH_2 sq acid), 2.13 (m, 1H, H-8), 2.03 (m, 16H, CH_2 sq), 1.97 (m, 1H, H-20), 1.82 (m, 1H, H-20), 1.71 (m, 18H, C(sq)-CH_3), 1.29 (d, 3H, CH_3); MS (ESI+) *m/z* (%): 926.14 (100) [MH^+].

2.5. Synthesis of 2'-trisnorsqualenoyl paclitaxel ester (SQptx)

2'-trisnorsqualenoyl paclitaxel ester (**8**) was prepared by chemoselective esterification of paclitaxel with 1,1',2-*tris*norsqualenoic acid (**1**) (Figure S2c). Paclitaxel (**7**) (1.2 g, 1.4 mmol), dissolved in 30 mL of dichloromethane, was reacted with EDAC (*N*-ethyl-*N'*-(3-dimethylaminopropyl) carbodiimide) (0.160 g, 0.84 mmol), in the presence of DMAP (4-dimethylaminopyridine) (0.034 g, 0.28 mmol) and 1,1',2-*tris*norsqualenoic acid (**1**)

(0.336 g, 0.84 mmol) previously dissolved in 5 mL of dichloromethane at room temperature. After 3 h, the reaction was stopped with water and extracted with brine. The crude mixture was purified on silica gel eluting with 5 to 20 % ethyl acetate in dichloromethane to give pure SQptx (**8**) as a white amorphous solid (1.123 g, 65 %). Characterization: 1H-NMR (300 MHz, $CDCl_3$) δ: 8.13 (d, 2H, C23, C27ArH), 7.75 (d, 2H, C39, C43 ArH), 7.62 (t, 1H, C25 ArH), 7.53-7.49 (band, 3H, C24, C26, C41 ArH), 7.43-7.35 (band, 7H, C33, C34, C35, C36, C37, C40, C42 ArH), 6.91 (d,1H, 4'NH), 6.35 (s, 1H, C(10)-H), 6.24 (m, 1H, C(13)-H), 5.99 (dd, 1H, C(3')-H), 5.69 (d, 1H, C(2)-H), 5.53 (d, 1H, C(2')-H), 5.20 (m, 5H, C(SQ-H)), 4.97 (d, 1H, C(5)-H), 4.44 (m, 1H, C(7)-H- 4.33 (d, 1H, C(20)-H_a), 4.20 (d, 1H, C(20)-H_b), 3.85 (d, 1H, C(3)-H), 2.55 (m, 1H, C(6)-H_a), 2.49 (s, 3H, C(29)-H), 2.45 (m, 2H, C$H_2$$CH_2$CO SQ), 2.30 (t, 2H, CH_2CH_2CO SQ), 2.23 (s, 3H, C(31)-H), 2.09 (s, 3H, C(18)-H), 2.00 (m, 16H, CH_2 SQ), 1.97 (m, 1H, C(6)-H_b), 1.70 (m, 1H, C(14)-H_a), 1.67 (s, 3H, C(19)-H), 1.61 (m, 18H, C(SQ)-CH_3), 1.25 (m, 1H, C(14)-H_b), 1.21 (s, 3H, C(16)-H), 1.13 (s, 3H, C(17)-H). MS (ESI+) *m/z* (%) 1237.24 (100) $[MH]^+$. Anal. Calcd for $C_{74}H_{93}NO_{15}$: C 71.88, H 7.58, N 1.13; found C 71.99, H 7.63, N 1.19.

2.6. Synthesis of (OC-6-33)-Diamminedichlorobis[4-(4,8,13,17,21-pentamethyl-docosa-4,8,12,16,20-pentaenylamino)-4-oxobutanoato]platinum(IV) (SQcis)

SQcis (**12**) was prepared by sequential treatment of cisplatin with hydrogen peroxide and succinic anhydride, followed by amide bond formation with 1,1',2-tris-norsqualenamine of the resulting platinum (IV) complex (**10**) (Figure S2d). To an ice-cooled solution of diaminebis(3-carboxypropanoato)dichloroplatinum (IV) (22) (128.6

mg, 0.24 mmol) in THF/DMF (v/v 5:1, 4 mL) was added dropwise triethylamine (61 mg, 0.60 mmol) and ethyl chloroformate (54.4 mg, 0.54 mmol, 2.1 equiv.). The reaction mixture was stirred at 0 °C for 30 min and a solution of 1,1',2-tris-norsqualenamine (240 mg, 0.62 mmol), 4-dimethylaminopyridine (5 mg, 0.04 mmol) in DMF (0.2 mL) was added. The resulting mixture was stirred at room temperature for 4 d. The solvents were removed under reduced pressure, and the residue was purified by column chromatography on silica gel eluting successively with AcOEt/MeOH: 98:2, and 95:5 to provide SQcis (**12**) (120 mg, 39 %) as a yellow oil. ^{1}H NMR(300 MHz, DMF-d_7) δ: 7.75 (t, J = 5.6 Hz, 2H, N*H*), 7.20-6.50 (m, 6H, NH_3), 5.25-5.00 (m, 10H), 3.15-3.05 (m, 4H, CH_2NHCO), 2.47 (t, J = 6.9 Hz, 4H), 2.37 (t, J = 6.4 Hz, 4H), 2.15-1.90 (m, 40H), 1.66 (s, 6H, $(CH_3)_2$C=), 1.61 (s, 18H, (CH_3)CH=), 1.59 (s, 12H, (CH_3)CH=); ^{195}Pt NMR (53.8 MHz, DMF-d_7) δ: 1174.4 (710 Hz); MS (ESI$^+$) *m/z* (%) = 1292.7 (100) $[M+23]^+$.

2.7. Synthesis of squalenoyl-DOTA Gd^{3+} complex ($SQGd^{3+}$)

Gd^{3+} is by far the most widely used contrast agent for MRI in clinic, because of their highest electronic spin value (S = 7/2). This high paramagnetism can yield a strong enhancement of the water proton relaxation rates, and this ability is assessed through the measurement of the relaxivity. In particular, the accessibility of water molecules to the magnetic center is a crucial factor to achieve good relaxivities.[3,4] In this respect, squalene-based nanoparticulate systems appear as promising candidates for MRI, as they possess water-filled inner channels due to their particular supramolecular organisation, in a hexagonal inverse phase (SQgem),[5] or in a cubic phase (squalenoyl zalcitabine, SQddc).[6] Therefore, we expected that the high number of water molecules contained in

the nanoparticles would result in a remarkable proton density surrounding the Gd^{3+}, necessary for high relaxivity

The squalenoyl-DOTA Gd^{3+} complex ($SQGd^{3+}$) was obtained in a seven-step process (Figure S2e). Briefly, 1,1',2-tris-nor-squalenic acid (**1**), easily available in four steps from squalene,[5] was first converted into 1,1',2,3-*tetranor*-squalenamine (**15**), through Curtius rearrangement of the acyl azide (**13**) and potassium hydroxide hydrolysis of the intermediate carabamate (**14**), with 62 % overall yield. The squalenamine was next acylated with bromoacetic acid using EDCI/DMAP as a coupling agent to give the key bromoacetamide (**16**), with 79 % yield. The coupling of (**16**) with the DO_3AEt macrocycle (**17**) was simply achieved by refluxing both (**16**) and (**17**) in acetonitrile with potassium carbonate as base providing (**18**) in 82 % yield. The final unmasking of the carboxylic groups in cyclen (**18**) was carried out by saponification of the three ester groups by lithium hydroxide to obtain the triacid (**19**) in 64 % yield. $SQGd^{3+}$ (**20**) was formed under pH-controlled conditions upon treatment of (**8**) with $GdCl_3$ at room temperature, with 58 % yield. The $SQGd^{3+}$ complex was thus obtained in a seven-step process from (**1**) and 14 % overall yield.

2.7.1. Synthesis of ethyl-(3,7,12,16,20-pentamethylhenicosa-3,7,11,15,19-pentaen-1-yl)-carbamate (**14**)

Distilled triethylamine (305 mg, 3 mmol) was a added to a stirred, ice-cooled solution of a 1,1',2-*trisnor*-squalenic acid (**1**) (1.0 g, 2.5 mmol) in anhydrous acetone (10 mL). Ethyl chloroformate (325 mg, 3 mmol) was added to this reaction mixture, and mechanical stirring was continued for 25 min at 0 °C. Then, a solution of sodium azide

(650 mg, 10 mmol) in distilled water (3 mL) was added dropwise over 5 min. After being stirred for 75 min at 0 °C, 10 mL of distilled water were added, and the reaction mixture was extracted with toluene (5 × 20 mL). The combined organic phases were dried over $MgSO_4$, filtered, and concentrated under reduced pressure, keeping the bath temperature < 40 °C to leave crude acyl azide (**13**) (1.5 g) as a colorless oil, which was used directly in the next step without further purification. IR (neat, cm^{-1}) ν: 2916, 2135, 1720, 1444.

A solution of the above acyl azide (**13**) (2.05 g, 5.12 mmol) in toluene (10 mL) and anhydrous ethanol (3 mL) was heated under reflux during 15 h. After cooling, the reaction mixture was concentrated under reduced pressure, and the residue was purified by column chromatography on silica gel eluting with a cyclohexane/AcOEt (4:1) to give carbamate (**14**) as a pale yellow oil (1.41 g, 62 % overall yield). IR (neat, cm^{-1}) ν: 2915, 1708, 1511, 1445, 1381, 1250; ^{1}H NMR (300 MHz, $CDCl_3$) δ: 5.20-5.05 (m, 5 H, =C*H*), 4.58 (broad s, 1 H, NH), 4.09 (q, *J* = 6.9 Hz, 2 H, OCH_2CH$_3$), 3.24 (m, 2 H, CONCH_2), 2.14 (t, *J* = 6.9 Hz, 2 H, CONCH$_2$CH_2), 2.15-1.90 (m, 16 H), 1.67 (s, 3 H, $(CH_3)_2$C=), 1.60 (s, 15 H, (CH_3)CH=), 1.23 (t, *J* = 6.9 Hz, 3 H, OCH$_2$CH_3); ^{13}C NMR (75 MHz, $CDCl_3$) δ: 156.5 (C), 135.1 (C), 134.7 (C), 134.6 (C), 131.5 (C), 131.0 (C), 127.0 (CH), 124.6 (CH), 124.4 (CH), 124.2 (2 CH), 60.6 (CH_2), 39.7 (2 CH_2), 39.6 (2 CH_2), 38.6 (CH_2), 28.1 (2 CH_2), 26.7 (CH_2), 26.6 (CH_2), 26.5 (CH_2), 25.7 (CH_3), 17.5 (CH_3), 16.0 (CH_3), 15.8 (2 CH_3), 15.5 (CH_3), 14.6 (CH_3); MS (APCI$^+$) *m/z* (%) = 444.4 (100) $[M+H]^+$; Anal. Calcd for $C_{29}H_{49}NO_2 \cdot H_2O$: C, 75.44, H, 11.13, N, 3.03. Found: C, 75.54, H, 10.8, N 3.03.

2.7.2. Synthesis of 3,7,12,16,20-pentamethyl-heneicosa-3,7,11,15,19-pentaenylamine (**15**)

The intermediate carbamate (**14**) (1.02 g, 2.31 mmol) was treated with an ethanolic solution of potassium hydroxide (30 mL, 30 mmol). The mixture was heated under reflux during 48 h. After cooling the reaction was concentrated under reduced pressure. The residue was taken in distilled water (10 mL) and extracted with diethyl ether (4 × 25 mL). The combined organic phases were dried over $MgSO_4$, filtered, and concentrated under vacuum. The residue was purified by flash column chromatography on silica gel eluting sequentially with cyclohexane: AcOEt/Et_3N (20:10:0.1), AcOEt/Et_3N (10:0.05), and AcOEt/MeOH/Et_3N (9:1:0.05) to provide 1,1',2,3-*tetranor*-squalenamine (**15**) as a pale yellow oil (766 mg, 89 % yield). IR (neat, cm^{-1}) ν: 2915, 2852, 1569, 1441, 1381; ^1H NMR (300 MHz, CD_3OD) δ: 5.28-5.04 (m, 5 H, =*CH*), 2.76 (t, *J* = 7.1 Hz, 2 H, N*CH*$_2$), 2.20-1.95 (m, 18 H), 1.70 (s, 3 H), 1.65 (s, 3 H), 1.63 (s, 12 H); ^{13}C NMR (75 MHz, CD_3OD) δ: 136.1 (C), 136.0 (C), 135.9 (C), 132.9 (C), 132.0 (C), 128.1 (CH), 125.7 (CH), 125.6 (CH), 125.5 (2 CH), 42.7 (CH_2), 40.9 (2 CH_2), 40.8 (CH_2), 40.2 (CH_2), 29.3 (2 CH_2), 27.9 (CH_2), 27.7 (CH_2), 27.6 (CH_2), 26.0 (CH_3), 17.8 (CH_3), 16.3 (3CH_3), 15.9 (CH_3); MS (ESI^+) *m/z* (%) = 372.6 (100) $[M+H]^+$; Anal. Calcd for $C_{26}H_{45}N \cdot {}^2/_3H_2O$: C, 81.40, H, 12.17, N, 3.65. Found: C, 81.59, H, 11.67, N, 3.61.

2.7.3. Synthesis of 2-bromo-N-(3,7,12,16,20-pentamethyl-henicosa-3,7,11,15,19-pentaenyl)-acetamide (**16**)

Bromoacetic acid (348 mg, 2.50 mmol), EDCI·HCl (320 mg, 1.67 mmol), DMAP (32 mg, 0.26 mmol), and LiBr (300 mg, 3.5 mmol, added to minimized the bromide/chloride

exchange due to EDCI·HCl) were sequentially added under mechanical stirring to a solution of 1,1',2,3-*tetranor*-squalenamine (**15**) (0.618 g, 1.66 mmol) in CH_2Cl_2 (4 mL). After being stirred at 20.0 ± 0.5 °C for 16 h, water (10 mL) was added, and the reaction mixture was extracted with CH_2Cl_2 (3 × 20 mL). The combined organic phases were dried over $MgSO_4$, filtered, and concentrated under vacuum. The oily residue was purified by flash column chromatography on a silica gel eluting successively with cyclohexane/EtOAc (2:1) and EtOAc/MeOH (20:1) to yield bromoacetamide (**16**), as a pale yellow oil (645 mg, 79 % yield). IR (neat, cm^{-1}) ν: 2925, 2852, 1653, 1541, 1445, 1382; ^{1}H NMR (300 MHz, $CDCl_3$) δ: 6.51 (broad s, 1 H, N*H*CO), 5.25 (t, *J* = 6.6 Hz, 1 H, *H*C=C), 5.20-5.00 (m, 4 H *H*C=C), 3.86 (s, 2 H, BrC*H*$_2$), 3.40-3.30 (m, 2 H, OCNHC*H*$_2$), 2.20 (t, *J* = 6.6 Hz, 2 H, OCNHCH$_2$C*H*$_2$), 2.20-1.90 (m, 16 H), 1.67 (s, 3H), 1.62 (s, 3H), 1.59 (s, 12 H); ^{13}C NMR (75 MHz, $CDCl_3$) δ: 165.2 (C), 135.2 (C), 135.0 (C), 134.9 (C), 131.3 (2 C), 127.9 (CH), 124.6 (CH), 124.5 (CH), 124.4 (CH), 124.3 (CH), 39.8 (2 CH_2), 39.7 (CH_2), 38.8 (CH_2), 37.8 (CH_2), 29.5 (CH_2), 28.4 (2 CH_2), 27.0 (CH_2), 26.9 (CH_2), 26.7 (CH_2), 25.8 (CH_3), 17.8 (CH_3), 16.1 (3 CH_3), 15.6 (CH_3); MS (APCI$^+$) *m/z* (%) = 494.2 (90) and 492.2 (100) $[M+H]^+$; Anal. Calcd for $C_{28}H_{46}BrNO$: C, 68.27, H, 9.41, N, 2.84. Found: C, 67.82, H, 9.52, N, 2.91.

2.7.4. Synthesis of triethyl-2,2',2''-[10-(2-oxo-2-{[3,7,12,16,20-pentamethylhenicosa-3,7,11,15,19-pentaen-1-yl]amino}ethyl)-1,4,7,10-tetraazacyclododecane-1,4,7-triyl]-triacetate (**18**)

A mixture of bromoacetamide (**16**) (626 mg, 1.27 mmol), macrocycle (DO_3AEt) (**17**) (500 mg, 1.16 mmol), and potassium carbonate (200 mg, 1.45 mmol) in anhydrous

acetonitrile (3 mL) was heated at 60.0 ± 0.5 °C for 24 h. After cooling, the reaction was filtered, and the solid was thoroughly washed with CH_2Cl_2, and the filtrate was concentrated under vacuum. The residue was purified by column chromatography on a silica gel, eluting successively with CH_2Cl_2/EtOH/Et_3N (9:1:0.05), and CH_2Cl_2/EtOH/Et_3N (4:1:0.02) to obtain the triester (**18**) as pale yellow viscous oil (802 mg, 82 % yield). IR (neat, cm^{-1}) ν: 3500-3000, (broad, NHCO), 2913, 2844, 1733, 1661, 1554, 1451, 1380, 1306, 1204, 1106; ^{1}H NMR (300 MHz, C_6D_6) δ: 10.14 (t, *J* = 5.2 Hz, 1 H, N*H*CO), 5.47-5.30 (m, 5 H, C=C*H*), 4.19-4.05 (m, 8 H, OC*H*$_2$CH$_3$), 3.90-2.00 (m, 42 H), 1.79 (s, 3 H), 1.78 (s, 3 H), 1.75 (s, 3 H), 1.74 (s, 3 H), 1.72 (s, 3 H), 1.67 (s, 3H), 1.15 (t, *J* = 7.1 Hz, 6H), 1.08 (t, *J* = 7.1 Hz, 3H); ^{13}C NMR (75 MHz, C_6D_6) δ: 174.8 (C), 173.2 (2 C), 172.7 (C), 135.5 (C), 135.1 (C), 134.9 (C), 133.4 (C), 131.0 (C), 125.8 (CH), 124.9 (2 CH), 124.8 (CH), 124.4 (CH), 60.9 (3 CH_2), 57.1 (CH_2), 55.6 (3 CH_2), 53-49 (m broad, 8 CH_2,), 40.3 (CH_2), 40.2 (2 CH_2), 39.8 (CH_2), 38.6 (CH_2), 27.8 (2 CH_2), 27.5 (CH_2), 27.2 (CH_2), 27.1 (CH_2), 25.8 (CH_3), 17.7 (CH_3), 16.3 (CH_3), 16.2 (CH_3), 16.1 (2CH_3), 14.3 (2 CH_3), 14.6 (CH_3); MS (ESI$^+$) *m/z* (%) = 865.3 (100) $[M+Na]^+$.

2.7.5. Synthesis of 2,2',2''-[10-(2-oxo-2-{[3,7,12,16,20-pentamethylhenicosa-3,7,11,15,19-pentaen-1-yl]amino}ethyl)-1,4,7,10-tetraazacyclododecane-1,4,7-triyl]triacetic acid (**19**)

To a carefully degassed solution of the triester (**18**) (564 mg, 0.665 mmol) in a 2:1 methanol/THF mixture (15 mL) was added dropwise a solution of lithium hydroxide (110 mg, 2.6 mmol) in water (2 mL). After stirring 15 h at room temperature, the reaction mixture was concentrated under reduced pressure. The residue was suspended in water

(15 mL) and neutralized with HCl 3 N. The obtained solution was dialyzed against water with a cellulose ester dialysis membrane (MWco= 500 Da) during 24 h. Finally, the solution was freeze dried to give triacid (**19**) as an amorphous white solid (327 mg, 64 % yield). IR (neat, cm^{-1}) ν: 3600-2900 broad, 1680-1580, 1400, 1220, ^{1}H NMR (400 MHz, CD_3OD) δ: 5.3-5.0 (m, 5 H, C=C*H*), 4.01-2.14 (m, 28 H), 2.13-1.91 (m, 16 H, CH_2), 1.69-1.55 (m, 18 H, C=C(CH_3)); ^{13}C NMR (100 MHz, CD_3OD) δ: 178-177 (3 C), 172.6 (C), 136.1 (C), 136.0 (C), 135.9 (C), 133.5 (C), 132.1 (C), 127.3 (CH), 125.7 (CH), 125.6 (2 CH), 125.5 (CH), 59.6-58.4 (m, 4 CH_2), 53-50.5 (m, 8 CH_2), 40.9 ($2CH_2$), 40.3 (CH_2), 39.3 (2 CH_2), 29.3 (2 CH_2), 28 (CH_2), 27.9 (CH_2), 27.6 (CH_2), 26 (CH_3), 17.9 (CH_3), 16.5-16.0 (4 CH_3); MS (ESI^+) *m/z* (%) = 794.8 (100) $[M+K]^+$, 779.8 (45) $[M+Na]^+$.

2.7.6. Synthesis of gadolinium 2,2',2''-[10-(2-oxo-2-{[3,7,12,16,20-pentamethylhenicosa-3,7,11,15,19-pentaen-1-yl]amino}ethyl)-1,4,7,10-tetraazacyclododecane-1,4,7-triyl]triacetic ($SQGd^{3+}$ complex) (**20**)

Gadolinium chloride hexahydrate $GdCl_3 \cdot 6H_2O$ (87 mg, 0.23 mmol) in water (1 mL) was added dropwise to 3 mL of an aqueous solution of the triacid (**19**) (174 mg, 0.23 mmol). The pH of the solution was continuously adjusted with NaOH 1 N to 6-7. The reaction mixture was stirred during 48 h at room temperature. The solution was then dialyzed against water with a cellulose ester dialysis membrane (MWco= 500 Da) during 24 h, and freeze dried. The white powder obtained (161 mg) was further purified by reversed-phase column chromatography on a C-18 grafted silica gel eluting with methanol. The collected fractions were analyzed using RP18 (F_{254}) silica gel TLC plate, and visualised with I_2. The suitable fractions were combined and eluted through a column

packed with chelex100 (sodium form), and the pH was kept between 6 and 7 with amberlite IR 120-H form. The absence of free Gd^{3+} ions was checked by using a xylenol orange indicator.[7] The fractions containing the pure $SQGd^{3+}$ complex (**20**) was collected and concentrated under vacuum. The resulting solid was taken up into water, and the solution (15 mL) was then freeze dried to collect the $SQGd^{3+}$ complex (**20**) as an amorphous white solid (122 mg, 58 % yield). The purity of the complex was > 92 % as determined by the Evans' method,[8,9] and by inductive coupled plasma atomic emission spectra (ICP-AES).[10] IR (neat, cm^{-1}) ν: 2925, 1602, 1384, 1086, 720; MS (ESI^+) *m/z* (%): 919.7 (30) $[M+Li]^+$; 935.7 (100) $[M+Na]^+$; 951.6 (10) $[M+K]^+$ (Figure S3); HRMS Calcd for $C_{42}H_{69}GdN_5O_7$ $[M + H]^+$: 913,4438; found: 913.4478.

2.8. Determination of the critical micelle concentration (CMC) of the $SQGd^{3+}$ complex

The CMC of the $SQGd^{3+}$ complex was determined by fluorescence spectroscopy using pyrene, a hydrophobic fluorescence probe that preferentially partitions into the hydrophobic core of the $SQGd^{3+}$ micelle. Briefly, a pyrene-saturated aqueous solution was prepared by mechanical stirring of a pyrene aqueous suspension overnight, followed by filtration to remove the excess of undissolved pyrene microcrystals. A $SQGd^{3+}$ complex stock solution (5 g/L) was prepared in pyrene-saturated aqueous solution, which was left to equilibrate under agitation during 1 day protected from light. Subsequently, the $SQGd^{3+}$ complex stock solution was diluted with pyrene-saturated water to obtain solutions of varying concentrations (from 10^{-3} to 5 g/L), which were further equilibrated under agitation during 1 day. The changes in the ratio of the pyrene excitation fluorescence intensities at 333 nm (I_{333}, for pyrene in water) and at 336 nm (I_{336}, for

pyrene within the hydrophobic micelle core) were monitored.[11] Fluorescence spectra were measured at thermostatized 23.0 ± 0.5 °C with a Perkin-Elmer LS-50B (Beaconsfield, Bucks, UK) computer-controlled luminescence spectrometer with FL WinLab software. The excitation spectra were measured at the emission wavelength (390 nm).

Following this method,[12] the excitation spectrum undergoes a small shift to longer wavelengths as the probe passes from a hydrophilic to a hydrophobic environment. This shift is quantified in terms of I_{336}/I_{333} ratio. The intensities ratios of pyrene fluorescence were plotted against the logarithm of $SQGd^{3+}$ complex concentration in aqueous solutions, obtaining a sigmoid curve (Figure S4). The CMC value was determined from the intersection of two straight lines: the horizontal line corresponding to low $SQGd^{3+}$ concentrations with an almost constant I_{336}/I_{333} value, and the line approximating the steep upward section of the sigmoidal curve. The estimated CMC value for the $SQGd^{3+}$ complex was 9.8 μmol.

2.9. Preparation of squalenoyl antitumor prodrug nanoparticles and nanomagnetite/squalenoyl antitumor prodrug composite nanoparticles

2.9.1. Preparation of SQgem nanoparticles and nanomagnetite/SQgem composite nanoparticles (USPIO/SQgem NPs)

Synthesis of SQgem nanoassemblies (average diameter and polydispersity index: 110 ± 25 nm and 0.179, respectively) was carried out by nano-precipitation.[2] Briefly, SQgem was dissolved in ethanol (2 mg/mL) and added dropwise under mechanical stirring (500 rpm, at 25.0 ± 0.5 °C) into a 10^{-5} N HCl aqueous solution, containing pluronic® F-68

(1 %, w/v) and dextrose (5 %, w/v). Under these conditions, the precipitation of SQgem NPs occurred spontaneously. Then, ethanol was evaporated under vacuum at 37.0 ± 0.5 °C using a Buchi Rotavapor® (Switzerland) rotary evaporator. NPs were then resuspended in fresh water up to a final volume of 2 mL. The final SQgem aqueous suspensions (2 mg/mL) contained a 5 % (w/v) of dextrose and a 1 % (w/v) of pluronic® F-68. For the characterization experiments, the NPs were freshly prepared and used within 24 h (conservation at 4.0 ± 0.5 °C).

The procedure followed for the synthesis of USPIO/SQgem NPs was similar to that described above for the SQgem NPs, except that SQgem was dissolved in an ethanolic suspension of magnetite nanocrystals (USPIO), prior to nano-precipitation in water. Practically, SQgem was dissolved in a 0.15 % (w/v) USPIO ethanolic suspension (2 mg/mL) and was added dropwise, under mechanical stirring (500 rpm, at 25.0 ± 0.5 °C), to 2 mL of an aqueous medium containing 10^{-5} N HCl, pluronic® F-68 (1 %, w/v) and dextrose (5 %, w/v). Cleaning of the USPIO/SQgem composite NPs was achieved by repeated magnetic separation and re-dispersion in an aqueous medium containing pluronic® F-68 (1 %, w/v) and dextrose (5 %, w/v), until the supernatant was transparent and its conductivity indicated that the suspensions were clean of both unreacted chemicals and non-magnetic particles (≤ 10 µS/cm). For the current investigation, the composite NPs were freshly prepared and used within 24 h (conservation at 4.0 ± 0.5 °C).

2.9.2. Preparation of SQdox nanoparticles and nanomagnetite/SQdox composite nanoparticles (USPIO/SQdox NPs)

Synthesis of SQdox nanoassemblies (average diameter and polydispersity index: 130 ± 20 nm and 0.134, respectively) was done by nano-precipitation. Briefly, SQdox was dissolved in a mixture of 0.1 mL ethanol and 0.2 mL of tetrahydrofuran. This solution was added dropwise under mechanical stirring (500 rpm, at 25.0 ± 0.5 °C) into a 10^{-5} N HCl aqueous solution, containing pluronic® F-68 (1 %, w/v) and dextrose (5 %, w/v). Under these conditions, the precipitation of SQdox NPs occurred spontaneously. Then, the organic solvents were evaporated under vacuum at 37.0 ± 0.5 °C using a Buchi Rotavapor® (Switzerland) rotary evaporator. NPs were then resuspended in fresh water up to a final volume of 2 mL. The final SQdox aqueous suspensions (2 mg/mL) contained a 5 % (w/v) of dextrose and a 1 % (w/v) of pluronic® F-68. For the characterization experiments, the NPs were freshly prepared and used within 24 h (conservation at 4.0 ± 0.5 °C).

The synthesis of USPIO/SQdox NPs was similar to that described above for the SQdox NPs, except that SQdox was dissolved in a 0.15 % (w/v) USPIO organic suspension (prepared with 0.1 mL ethanol and 0.2 mL of tetrahydrofuran), prior to nano-precipitation in water. This suspension was added dropwise, under mechanical stirring (500 rpm, at 25.0 ± 0.5 °C), to 2 mL of an aqueous medium containing 10^{-5} N HCl, pluronic® F-68 (1 %, w/v) and dextrose (5 %, w/v). Cleaning of the USPIO/SQdox composite NPs was achieved by repeated magnetic separation and re-dispersion in an aqueous medium containing pluronic® F-68 (1 %, w/v) and dextrose (5 %, w/v), until the supernatant was transparent and its conductivity indicated that the suspensions were clean of both unreacted chemicals and non-magnetic particles (≤

10 µS/cm). For the current investigation, the core/shell NPs were freshly prepared and used within 24 h (conservation at 4.0 ± 0.5 °C).

2.9.3. Preparation of SQptx nanoparticles and nanomagnetite/SQptx composite nanoparticles (USPIO/SQptx NPs)

Synthesis of SQptx nanoassemblies (average diameter and polydispersity index: 140 ± 30 nm and 0.148, respectively) was carried out by nano-precipitation. Briefly, SQptx was dissolved in ethanol (2 mg/mL) and added dropwise under mechanical stirring (500 rpm, at 25.0 ± 0.5 °C) into a 10^{-5} N HCl aqueous solution, containing pluronic® F-68 (1 %, w/v) and dextrose (5 %, w/v). Under these conditions, the precipitation of SQptx NPs occurred spontaneously. Then, ethanol was evaporated under vacuum at 37.0 ± 0.5 °C using a Buchi Rotavapor® (Switzerland) rotary evaporator. NPs were then resuspended in fresh water up to a final volume of 2 mL. The final SQptx aqueous suspensions (2 mg/mL) contained a 5 % (w/v) of dextrose and a 1 % (w/v) of pluronic® F-68. For the characterization experiments, the NPs were freshly prepared and used within 24 h (conservation at 4.0 ± 0.5 °C).

The procedure followed for the synthesis of USPIO/SQptx NPs was similar to that described above for the SQptx NPs, except that SQptx was dissolved in an USPIO ethanolic suspension, prior to nano-precipitation in water. Practically, SQptx was dissolved in a 0.15 % (w/v) USPIO ethanolic suspension (2 mg/mL) and was added dropwise, under mechanical stirring (500 rpm, at 25.0 ± 0.5 °C), to 2 mL of an aqueous medium containing 10^{-5} N HCl, 1 % (w/v) pluronic® F-68 and5 % (w/v) dextrose. Cleaning of the USPIO/SQptx NPs was achieved by repeated magnetic

separation and re-dispersion in an aqueous medium containing pluronic® F-68 (1 %, w/v) and dextrose (5 %, w/v), until the supernatant was transparent and its conductivity indicated that the suspensions were clean of both unreacted chemicals and non-magnetic particles (≤ 10 μS/cm). For the current investigation, the composite NPs were freshly prepared and used within 24 h (conservation at 4.0 ± 0.5 °C).

2.9.4. Preparation of SQcis nanoparticles and nanomagnetite/SQcis composite nanoparticles (USPIO/SQcis NPs)

Synthesis of SQcis nanoassemblies (average diameter and polydispersity index: 125 ± 15 nm and 0.124, respectively) was done by nano-precipitation. Briefly, SQcis was dissolved in DMF (2 mg/mL) and added dropwise under mechanical stirring (500 rpm, at 25.0 ± 0.5 °C) into a 10^{-5} N HCl aqueous solution, containing pluronic® F-68 (1 %, w/v) and dextrose (5 %, w/v). Under these conditions, the precipitation of SQcis NPs occurred spontaneously. Then, DMF was removed by dialysis against water with a cellulose ester dialysis membrane (MWco= 500 Da) during 24 h. NPs were then resuspended in fresh water up to a final volume of 2 mL. The final SQcis aqueous suspensions (2 mg/mL) contained a 5 % (w/v) of dextrose and a 1 % (w/v) of pluronic® F-68. For the characterization experiments, the NPs were freshly prepared and used within 24 h (conservation at 4.0 ± 0.5 °C).

The procedure followed for the synthesis of USPIO/SQcis NPs was similar to that described above for the SQcis NPs, except that SQcis was dissolved in a 0.15 % (w/v) DMF suspension of USPIO, prior to nano-precipitation in water. This suspension was added dropwise, under mechanical stirring (500 rpm, at 25.0 ± 0.5 °C), to 2 mL of an

aqueous medium containing 10^{-5} N HCl, pluronic® F-68 (1 %, w/v) and dextrose (5 %, w/v). Cleaning of the USPIO/SQcis composite NPs was achieved by repeated magnetic separation and re-dispersion in an aqueous medium containing pluronic® F-68 (1 %, w/v) and dextrose (5 %, w/v), until the supernatant was transparent and its conductivity indicated that the suspensions were clean of both unreacted chemicals and non-magnetic particles (≤ 10 µS/cm). For the current investigation, the nanocomposites were freshly prepared and used within 24 h (conservation at 4.0 ± 0.5 °C).

2.10. Preparation of $SQGd^{3+}$ micelles and SQgem/$SQGd^{3+}$ composite nanoparticles

Remarkably, the newly synthesized $SQGd^{3+}$ contrast agent spontaneously formed micelles (average diameter ≈ 7 nm) in water whatever its concentration (0.1 - 80 mg/mL). This was achieved by mixing under magnetic stirring the $SQGd^{3+}$ powder in water.

The composite SQgem/$SQGd^{3+}$ NPs were prepared by dissolving 4 mg SQgem in 0.5 mL of a 0.1 % (w/v) $SQGd^{3+}$ ethanolic solution. This solution was then added dropwise, under mechanical stirring (500 rpm, at 25.0 ± 0.5 °C) into 1 mL of water. Ethanol was evaporated under vacuum at 37.0 ± 0.5 °C using a Buchi Rotavapor® (Switzerland) rotary evaporator. For the characterization experiments, the NPs were freshly prepared and used within 24 h (conservation at 4.0 ± 0.5 °C).

2.11. Characterization of the nanomagnetite/squalenoyl antitumor prodrug composite nanoparticles

2.11.1. Geometry

Mean particle diameters were determined in triplicate at 25.0 ± 0.5 ºC by photon correlation spectroscopy (PCS) using a Malvern Autosizer® 4700 (Malvern Instruments Ltd., UK). The scattering angle was set at 60°, and the measurement was made after suitable dilution of the aqueous nanoparticle suspensions (≈ 0.1 %, w/v), that were previously sonicated for 5 min. Using the PCS technique, the instrument evaluates the autocorrelation function of the scattered light intensity; in its standard mode of operation, the software provides an average diameter and a polydispersity index based on the second-order cumulant procedure.

To confirm the size measurements and to carry out a preliminary inspection of the coating efficacy, the size and shape of the NPs (*i.e.*, USPIO, SQgem, SQdox, SQptx, SQcis, USPIO/SQgem, USPIO/SQdox, USPIO/SQptx, and USPIO/SQcis) were checked through analysis by high resolution transmission electron microscopy (HRTEM), obtained using a STEM PHILIPS CM20 (The Netherlands) high resolution transmission microscope set at 80 kV accelerating voltage. Prior to observation, dilute suspensions (≈ 0.1 %, w/v) were sonicated for 5 min, and drops were placed on copper grids with formvar film. The grids were then dried at 35.0 ± 0.5 ºC in a convection oven.

2.11.2. Drug loading

The amount of squalenoyl prodrug actually bound to the corresponding USPIO/SQgem, USPIO/SQdox, USPIO/SQptx, and USPIO/SQcis nanocomposite was obtained from the weight difference between the coated nanocomposites and the bare USPIO particles. Drug incorporation to these core/shell NPs was expressed in terms of

drug loading (%), *e.g.*, gemcitabine loading: (encapsulated gemcitabine (mg) / USPIO/SQgem carrier (mg)) × 100.[13]

The nanocomposites were characterized by extremely high drug loadings compared to the currently available nanocarriers. Concretely, the following drug payload were achieved: 24 wt % gemcitabine loading (as compared with 5.9 % into liposomes,[14] and 7.6 % into polymeric NPs[15]), 23.2 wt % doxorubicin loading (as compared with 25 % into liposomes,[16] and 2.2 % into polymeric NPs[17]), 22.4 wt % paclitaxel loading (as compared with 3 % into liposomes,[18] and 5.5 % into polymeric NPs[19]), and 23.5 wt % cisplatin loading (maximum of 10 % into liposomes,[20] and 0.98 % into polymeric NPs[21]).

2.11.3. Surface electrical and thermodynamic properties

The squalenoyl prodrug shell of the USPIO/SQgem, USPIO/SQdox, USPIO/SQptx, and USPIO/SQcis (core/shell) NPs was qualitatively confirmed by the analysis of the electrokinetic properties of the colloids. Since the surface properties of USPIO NPs, due to the nature of their charge generating groups, are extremely sensitive to pH variations in contrast to squalenoyl antitumor prodrug NPs, we tested the influence of the pH on the zeta potential (ζ) of the three kinds of colloids [*i.e.*, USPIO, squalenoyl antitumor prodrug NPs (SQgem, SQdox, SQptx, and SQcis), and USPIO/squalenoyl antitumor prodrug composite NPs (USPIO/SQgem, USPIO/SQdox, USPIO/SQptx, and USPIO/SQcis)] in the presence of 10^{-3} M NaCl. ζ was also measured as a function of [NaCl] at a constant pH of 5.6. Hence, the surface electrical properties of the different colloids [≈ 0.1 % (w/v) aqueous suspensions] were analyzed using a Malvern Zetasizer 2000 electrophoresis device (Malvern Instruments Ltd., UK). Measurements were

performed at 25.0 ± 0.5 ºC, after 24 h of contact at this temperature under mechanical stirring (50 rpm). The experimental uncertainty of the measurements was below 5 %. The theory of O'Brien and White was used to convert the electrophoretic mobility (u_e) into zeta potential (ζ) values.[22]

It was concluded that the deposition of the squalenoyl prodrugs around the USPIO had effectively taken place, since the ζ – pH and ζ – ionic strength trends of the nanomagnetite/squalenoyl antitumor prodrug composite NPs were almost identical to those of the pure squalenoyl antitumor prodrug NPs, and because pure magnetic NPs displayed a very different electrical profile (see supporting Figures 5 and 6). The thermodynamic analysis was in agreement with the electrokinetic characterization, suggesting that the surface coverage of USPIO by the squalenoyl antitumor prodrugs was complete, since the components of γ_S for nanomagnetite/squalenoyl antitumor prodrug composites coincided well with those of pure squalenoyl prodrugs (see supporting Figure 7b). Furthermore, the hydrophilic nature of USPIO turned into hydrophobic (similar to that of the pure SQgem, SQdox, SQptx, and SQcis) when entrapped into the pure squalenoyl antitumor prodrugs (see supporting Figure 8). This electrokinetic characterization helped to investigate the mechanism by which USPIO were so efficiently implanted into the squalenoyl antitumor prodrug nanoassemblies: in the acidic conditions (pH ≈ 5) used for the synthesis of magnetic nanocomposites, an attractive electrostatic interaction between the positively charged USPIO and the negatively charged squalenoyl antitumor prodrugs allowed the enrichment of the USPIO surface by SQgem, SQdox, SQptx, or SQcis (see Figure S5 in supporting information).

The differences between the surface properties of the three kinds of NPs [USPIO, squalenoyl antitumor prodrug NPs (SQgem, SQdox, SQptx, and SQcis), and USPIO/squalenoyl antitumor prodrug composite NPs (USPIO/SQgem, USPIO/SQdox, USPIO/SQptx, and USPIO/SQcis)] were ascertained by the investigation of their surface free energy components (γ_S^{LW}, γ_S^+, γ_S^-). This study started by measuring the contact angles with three probe liquids [water (γ_L^{LW} = 21.8 mJ/m^2, $\gamma_L^+ = \gamma_L^-$ = 25.5 mJ/m^2), diiodomethane (γ_L^{LW} = 50.8, $\gamma_L^+ = \gamma_L^-$ = 0 mJ/m^2), and formamide (γ_L^{LW} = 39.0 mJ/m^2, γ_L^+ = 2.28 mJ/m^2, γ_L^- = 39.6 mJ/m^2). All γ_L data were taken from van Oss][25] for these materials at 25.0 ± 0.5 ºC inside a thermostatic chamber, using a Ramé-Hart 100-00 goniometer (USA) with a CCD camera and a digital image analysis of drop pictures. Pellets (1.3 cm radius) of the powdered dry solids were prepared by compression in a Spepac (UK) hydraulic press set to 8 Ton during 5 min. At least 10 droplets were placed on the particle pellets, and the average contact angle and standard deviation were measured. Significant differences were observed between pure USPIO and USPIO/squalenoyl antitumor prodrug composite NPs (Figure S7a). However, it is the evaluation of the γ_S components that provided the best physical information about the surface thermodynamics of the NPs. This investigation was done by performing a surface thermodynamic analysis following the model proposed by van Oss.[25] The model starts from the separation of γ_S into two components, γ_S^{LW} and γ_S^{AB}, accounting for the van der Waals and acid/base interfacial interactions:

$$\gamma_S = \gamma_S^{LW} + \gamma_S^{AB} \quad (1)$$

and the acid/base component is in turn considered as a harmonic mean of two additional quantities, γ_S^+ and γ_S^-, known, respectively as electron acceptor and electron donor components. Thus, the polar contribution to the surface free energy is controlled by the tendency of the solid to accept or give electrons:

$$\gamma_S^{AB} = 2\sqrt{\gamma_S^+ \gamma_S^-} \tag{2}$$

The same applies to the liquid (or any other) phase present in the suspension and, most important, to the solid/liquid interfacial free energy:

$$\gamma_{SL}^{TOT} = \gamma_{SL}^{LW} + \gamma_{SL}^{AB} \tag{3}$$

$$\gamma_{SL}^{LW} = \left(\sqrt{\gamma_S^{LW}} - \sqrt{\gamma_L^{LW}}\right)^2 = \gamma_S^{LW} + \gamma_L^{LW} - 2\sqrt{\gamma_S^{LW}\gamma_L^{LW}}$$

$$\gamma_{SL}^{AB} = 2\left(\sqrt{\gamma_S^+\gamma_S^-} + \sqrt{\gamma_L^+\gamma_L^-} - \sqrt{\gamma_S^+\gamma_L^-} - \sqrt{\gamma_S^-\gamma_L^+}\right) = 2\left(\sqrt{\gamma_S^+} - \sqrt{\gamma_L^+}\right)\left(\sqrt{\gamma_S^-} - \sqrt{\gamma_L^-}\right)$$

If we now imagine a drop of liquid in equilibrium on a molecularly flat solid surface, the contact angle θ can be related to the *LW* and *AB* components of γ_S and γ_L,[25] through Young's equation:

$$2\sqrt{\gamma_S^{LW}\gamma_L^{LW}} + 2\sqrt{\gamma_S^+\gamma_L^-} + 2\sqrt{\gamma_S^-\gamma_L^+} = \gamma_L(1+\cos\theta) \tag{4}$$

Note that if γ_L^{LW}, γ_L^+, γ_L^- are known for three probe liquids (water, diiodomethane and formamide), and their corresponding contact angles are measured (Figure S7a), a system of three equations like eq. (4) can be formulated, the solution of which yields the unknowns γ_S^{LW}, γ_S^+, γ_S^-. This evaluation of the γ_S components provides the best physical information about the surface thermodynamics of the materials (Figure S7b). These changes in the surface free energy manifest themselves in the lyophobicity/lyophilicity characteristics of the different materials. According to van

Oss,[25] the free energy of interaction (not considering the electrostatic component) between the solid phases immersed in the liquid can be written as follows in terms of the total interfacial tension between phases *S* and *L* [eq. (3)]:

$$\Delta G_{SLS}^{TOT} = -2\gamma_{SL}^{TOT} \quad (5)$$

This gives a quantitative indication of the lyophobic/lyophilic nature of the solid: if it happens to be negative, interfacial interactions favour attraction of the particles to each other, and they are considered lyophobic (hydrophobic in aqueous media). Lyophilicity (hydrophilicity in aqueous media) will correspondingly be associated to positive values of ΔG_{SLS}^{TOT}. Figure S8 shows that the hydrophilic nature of USPIO turned into hydrophobic (similar to that of the pure squalenoyl antitumor prodrug NPs) when coated by SQgem, SQdox, SQptx, or SQcis. Thus, the thermodynamic analysis was in agreement with the electrokinetic characterization, suggesting that the surface coverage of USPIO by the squalenoyl antitumor prodrugs was complete.

Furthermore, thermodynamic arguments can also be given to explain the mechanism by which USPIO were so efficiently implanted into the squalenoyl antitumor prodrug nanoassemblies. From γ_S data (see supporting Figure 7b), the free energy ΔG_{MAS}, of the interaction between USPIO (*M*) and the squalenoyl antitumor prodrugs (*S*) in the aqueous medium (*A*) could be calculated by using the Dupré equation:[25,27]

$$\Delta G_{MAS} = \gamma_{MS} - \gamma_{MA} - \gamma_{SA} \quad (6)$$

where the interfacial free energies are given by eq. (3) for each pair of interfaces involved. The results of the calculation were -10.3 ± 0.8 mJ/m^2 (USPIO/SQgem), -18.6 ± 1.3 mJ/m^2 (USPIO/SQdox), -5.2 ± 0.4 mJ/m^2 (USPIO/SQptx), and -12.4 ± 1.1 mJ/m^2 (USPIO/SQcis) meaning that the van der Waals and acid-base interactions between the

USPIO and the squalenoyl antitumor prodrugs were neatly attractive. In other words, it was thermodynamically favourable for SQgem, SQdox, SQptx, or SQcis to remain adsorbed onto USPIO NPs rather than as isolated entities in water.

2.11.4. Magnetic properties

The magnetic properties of nanomagnetite and nanomagnetite/squalenoyl antitumor prodrug composite nanoparticles were determined using a Manics DSM-8 vibrating magnetometer (France) at 25.0 ± 0.5 ºC. Almost no hysteresis was observable (Figure S9a), as expected from the superparamagnetic character of nanomagnetite. The magnetic properties of nanomagnetite agree with those previously reported in the literature.[28] From the linear portions (low field) of the curves in this figure, we could estimate the initial susceptibility (χ_i) for USPIO, USPIO/SQgem, USPIO/SQdox, USPIO/SQptx, and USPIO/SQcis. It was respectively determined to be equal to 0.15 ± 0.01, 1.94 ± 0.19, 2.13 ± 0.09, 1.86 ± 0.12, 2.08 ± 0.07.

The field-responsive behaviour of the nanomagnetite/squalenoyl antitumor prodrug composites was qualitatively analyzed by both optical and microscope visualization of a 0.5 % (w/v) aqueous suspension using a 1.1 T permanent magnet close to the flat surfaces of glass vial containing composite particles. Microscope visualization was done using a Nikon SMZ800 (Japan) stereoscopic zoom microscope. No significant differences were observed between the high magnetic field-responsive behaviour of the composite NPs. For instance, Figure S9b shows the complete magnetic sedimentation of the USPIO/SQgem NPs in less than 5 min. Microscopic observations of the structures generated by placing the permanent magnet close to one face of a small drop of

USPIO/SQgem NPs suspension are shown in Figure S9c. Particle chaining in the field direction was an indication of strong magnetic dipolar interactions between the particles. Such interactions overcome the double layer repulsions and provide a useful tool in driving the SQgem-loaded particles to their place of action and, if required, concentrating them in a desired location.

Thus, all the prepared nanomagnetite/squalenoyl antitumor prodrug composite nanoparticles were characterized by very high drug loading and important magnetic susceptibility.

2.11.5. In vitro squalenoyl antitumor prodrug release from magnetic composite nanoparticles

SQgem, SQdox, SQptx, and SQcis release from USPIO/SQgem, USPIO/SQdox, USPIO/SQptx, and USPIO/SQgem NPs, respectively, was performed in PBS using the dialysis bag method (pH = 7.4 ± 0.1). The dialysis bag (having a cut-off of 2000 Da (Spectrum® Spectra/Por® 6 dialysis membrane tubing, USA)) retains the NPs and allows the free squalenoyl prodrug to be released into the dissolution medium. The bags were soaked in water for 12 h before use. Practically, 2 mL of nanomagnetite/squalenoyl antitumor prodrug composites suspension (containing 2 mg/mL of squalenoyl prodrug) was poured into the bag with the two ends fixed by clamps. The bags were placed in a beaker filled with 100 mL of the dissolution medium, and were stirred at 200 rpm. The temperature was maintained at 37.0 ± 0.5 ºC during all the release experiments, which were performed in triplicate. At different time intervals (0.08, 0.17, 0.25, 0.33, 0.5, 0.75, 1, 2, 3, 6, 9, and 12 h), 5 mL samples of the medium were withdrawn for UV-

Vis spectrophotometric analysis. An equal volume of PBS solution, maintained at the same temperature, was added after sampling to ensure sink conditions.

UV absorption measurements were carried out in a 8500 UV-Vis spectrophotometer (Dinko, Spain) to measure the squalenoyl antitumor prodrug release using quartz cells of 1 cm path length. Good linearity was observed at the maximum absorbance wavelengths and the method was validated and verified for accuracy, precision and linearity, demonstrating its reproducibility and the absence of molecular interactions. These parameters were studied in standard solutions in six replicates. Noteworthy, no traces of antitumor free drug were observed during the release experiment, showing that no burst release of the free drug occurred during this time interval.

As can be observed in Figure S10, the release of the squalenoyl antitumor prodrugs from the corresponding magnetic core/shell NPs was quite linear (zero order) during 2 h.

2.12. Visualization of USPIO/SQgem composites in solid tumors using MRI

Magnetic resonance imaging (MRI) measurements were performed using a horizontal 7 T bore magnet (Oxford, UK) interfaced by an Avance console (Bruker, Germany) and equipped with a 365 mT/m actively shielded gradient device (I.D. = 9 cm, Resonance Research Inc., MA, USA). A 38 mm-diameter birdcage coil was used for transmission and detection.

2.12.1. In vivo MRI protocol

All animal experimentations were conducted according to the French and European Community guidelines for the care and use of experimental animals. Four DBA/2 mice (4 – 5 weeks old) weighing ≈ 15 – 18 g were used for this study. The mice were provided with standard mouse food and water *ad libitum*. L1210 *wt* murine subcutaneous tumor model was developed by subcutaneous injection into the upper part of the right flank of mice, of the exponentially growing L1210 *wt* leukemia cells (1×10^6 cells) in suspension containing 30 % growth factor reduced Matrigel™. After waiting for 5 days, when mice developed palpable tumors at the injection site, they were examined by MRI before injection of USPIO/SQgem NPs. Then, the mice were injected intravenously with USPIO/SQgem (5 mg/Kg equivalent of gemcitabine) with (3 mice) or without (1 mouse) exposure to a 1.1 T extracorporeal magnetic field during 2 h. Afterwards, a new complete MRI examination was carried out. Practically, the anesthetized mice (using isoflurane 0.8 % in 50 % O_2 and 50 % N_2O) were immobilized and placed in horizontal position in a whole body mouse holder. Body temperature was monitored and kept at 37.0 ± 0.5 ºC using heated mattress. The animal was positioned using scouting gradient-echo images in the three-orthogonal directions and a low resolution 2D axial-Rapid Acquisition with Relaxation Enhancement (RARE) sequence, with the following parameters: repetition time (TR) of 2000 ms, effective echo time (TE) of 8 ms, RARE factor (rf) of 4, field of view (FOV) of 3.5 × 3.5 cm, acquisition matrix of 128 × 128, 25 contiguous 2 mm thick slices, and a number of averages (na) of 1. Then, 2 MRI sequences were used: a slightly T_2-weighted 2D axial RARE (TR: 2520 ms; TE: 19 ms; rf: 4; FOV: 3.5 × 3.5 cm; matrix size: 256 × 256; 41 contiguous 0.5 mm thick slices; and, na: 4), and a multi-echo-multi-slices sequence was used for T_2 measurement in the central part of the tumors (TR: 4000

ms; 8 TE values between 8 and 124 ms; rf: 4; FOV: 3.5 × 3.5 cm; matrix size: 128 × 128; 9 contiguous 1 mm thick slices; and, number of scans: 4). The total imaging time for each examination was ≈ 20 min.

2.12.2. MRI data analysis

As tumor is a very heterogeneous tissue, with variations of magnetic susceptibility, it was difficult to distinguish between signal variations due to the tissue heterogeneities or to the presence of NPs. Alternatively, T_2-weighted experiments using a spin-echo sequence succeeded in removing the effect of tumor heterogeneity. Thus, we used the T_2 contrast property of USPIO/SQgem composite NPs to carry out this study.

T_2-weighted images were analyzed using Paravision (Bruker, Germany). Tumors were manually segmented, and the images registered before and after treatment were analyzed in parallel, slice by slice. The volume of the tumor was calculated as the sum of its area in each slice multiplied by the slice thickness. These volumes were equal to 139 ± 3 mm^3 for mouse 1, 256 ± 3 mm^3 for mouse 2, 197 ± 3 mm^3 for mouse 3, and 357 ± 4 mm^3 for mouse 4. USPIO/SQgem NPs were T_2 contrast agents and when their concentration in a tissue increased, the apparent T_2 relaxation of the tissue decreased following the eq.:

$$\frac{1}{T_2^{(i)}} - \frac{1}{T_2^{(0)}} = r2C^{(i)} \tag{7}$$

where $T_2^{(0)}$ is the transversal relaxation time of the tissue without magnetic composites, and $T_2^{(i)}$ is the transversal relaxation time in a tissue containing a $C^{(i)}$ concentration of NPs. The comparison between T_2-weighted image after USPIO/SQgem NPs injection and

the corresponding T_2 map (Figure S11A), showed that a hypo-signal area corresponded effectively to a low T_2 area. In our experiments, we compared the tumor tissue before and after the injection of USPIO/SQgem NPs, and a decrease in intensity corresponded to a local increase in tissue NP concentration.

Each T_2-weighted slice of the tumor before treatment was used to define the class of hypo-intensity pixels ($p < 0.05$), and determined its upper threshold. This threshold was then used to define the hypo-intensity class pixels in the T_2-weighted corresponding slice of the tumor after treatment (Figure S11B). This hypo-intensity class was then divided in 2 classes. The volume of each class was determined as the sum of the hypo-intensity areas in each slice multiplied by the slice thickness. For comparison between the different mice, these volumes were then expressed as a percentage of the volume of the tumor.

2.13. Anticancer activity of USPIO/SQgem composite nanoparticles

The animal experiments were carried out according to the French and European Community guidelines for the care and use of experimental animals. DBA/2 mice (4 – 5 weeks old) weighing ≈ 15 – 18 g were used for this study. The mice were provided with standard mouse food and water *ad libitum*. L1210 *wt* murine subcutaneous tumor model was developed by subcutaneous injection into the upper part of the right flank of mice, of the exponentially growing L1210 *wt* leukemia cells (1×10^6 cells) in suspension containing 30 % growth factor reduced Matrigel™. After waiting for 5 days, when mice developed palpable tumors at the injection site, the mice were randomly divided into six groups of 6 each, *i.e.* untreated, treated with USPIO/squalene NPs (placebo), treated with gemcitabine (5 mg/Kg), treated with SQgem NPs (5 mg/Kg equivalent of gemcitabine),

treated with USPIO/SQgem NPs (5 mg/Kg equivalent of gemcitabine), and treated with USPIO/SQgem NPs under the influence of a 1.1 T extracorporeal magnetic field (5 mg/Kg equivalent of gemcitabine). All the groups of tumor bearing mice except untreated, were intravenously treated on days 6, 9, 13, and 16 after the implantation of tumors (a 4-dose intravenous bolus injection schedule). Following treatment, the mice were monitored regularly for differences in tumor volume reduction to assess the anticancer efficacy.

2.13.1. Tumor histology and immunohistochemistry studies

To further evidence the antitumor activity of the magnetic composite formulations, following completion of the treatment schedule, the tumors were isolated from mice and processed for histology examination. One mouse from each group [*i.e.*, untreated or treated either with SQgem NPs (5 mg/Kg equivalent of gemcitabine), USPIO/SQgem composites (no extracorporeal magnetic field, no-MF) (5 mg/Kg equivalent of gemcitabine), or USPIO/SQgem composites (with 1.1 T extracorporeal magnetic field for 2 h after injection, MF) (5 mg/Kg equivalent of gemcitabine)] was sacrificed and the tumor was isolated. The isolated tumors were fixed overnight in Finefix solution at 4.0 ± 0.5 ºC. Then, the tumors were sequentially treated with ethanol and toluene and fixed in paraffin. 3 μm sized paraffin embedded tumor sections were cut using microtome blade, fixed on the glass slide for overnight at 56.0 ± 0.5 °C in an oven.

The tumor sections were analyzed for histology by optical microscopy using the Hematoxylin-Eosin-Saffran (HES) staining technique. Briefly, paraffin embedded tumor sections were de-paraffinated by successive treatment with toluene and ethanol, and

finally washed with purified water. Then, the tumor sections were sequentially stained using hematoxylin, eosin and saffran by successive washings in water or ethanol and finally with toluene. Afterwards, the sections were mounted for observation under microscope.

Additionally, in order to differentiate the dead cells from the proliferating cell population in the tumor tissue, Ki-67 cell proliferation assay was performed using immunohistochemistry evaluation. Ki-67 is a nuclear antigen expressed in proliferating cells in the late G_1, S, G_2, and M phases but is absent in resting cells (G_0).[29] Purified mouse anti-human Ki-67 antibody (BD Biosciences Pharmingen, USA) was used for the demonstration of the Ki-67 antigen. Paraffin embedded tumor sections prepared from the untreated or treated tumors collected from mice, and human tonsil section as a positive control for Ki-67 antigen, were de-paraffinated by washing the sections with toluene, ethanol and purified water. Demasking of epitope was performed in citrate buffer at 85 – 90 °C. Then, the tumor sections were surrounded by hydrophobe circles using a hydrophobe marker. The endogenous peroxidases were blocked by incubating the tumor and tonsil sections using 0.3 % H_2O_2 solution. To prevent the non-selective binding of antibody, the tumor and tissue sections were incubated with normal horse serum (Vector Laboratories Inc., USA). Then, the above sections were incubated with anti-human Ki-67 antibody for 1 h, followed by incubation with anti-mouse IgG biotinylated antibody. To ensure specific staining of the Ki-67 positive cells, the tumor tissue sections were also treated separately with either first antibody or second antibody. The tumor and tonsil sections were washed with PBS and incubated with an avidin-biotin mixture for 30 min. Later, these sections were incubated with diaminobenzidene in dark for 10 min, washed

with PBS, coloured with hematoxylin and mounted on slides for observation under microscope. The labeled cells of three different slides of each tumor sample were counted under 40X magnification. The significance of difference between treatment groups was determined by the two-tailed Student's *t* test.

A considerably lower Ki-67 index (10 %) has been monitored in tumor sections of mice treated with USPIO/SQgem NPs under exposure to the external magnetic field, as compared to the other treatments (*i.e.*, 48 % Ki-67 index for tumors treated by SQgem NPs, and 45 % Ki-67 index for tumors treated by USPIO/SQgem NPs in the absence of the extracorporeal magnetic field). This highlight the superiority of magnetically-guided USPIO/SQgem NPs in wiping out the proliferating cancer cells from the tumor tissue (Figure S12).

2.13.2. Determination of USPIO in tumor biopsies of mice treated with USPIO/SQgem nanoparticles

The USPIO/SQgem NPs accumulated in the tumor tissue were qualitatively evaluated in terms of iron content using classical Prussian blue staining technique (Figure S13).[30] The reaction involves the treatment of tumor sections with acid solutions of ferrocyanides. The ferric ions (+3 form) present in the tumor tissue combines with the ferrocyanide and results in the formation of a bright blue pigment called Prussian blue. Briefly, the de-paraffinated tumor sections were hydrated in distilled water and immersed for 20 min into the freshly prepared mixture of equal parts of 20 % hydrochloric acid and 10 % potassium ferrocyanide solution. The tumor sections were then washed thrice in distilled water, and counter stained with nuclear fast red for 5 min. Finally, the sections

were rinsed twice with distilled water, alcohol 100 %, followed by xylene and mounted with cover slips for observation under optical microscope. In case of positive control for iron, the tumor section of untreated mice was incubated with an USPIO aqueous suspension (0.15 %, w/v) for 1 min, and then washed with distilled water and treated for Prussian blue staining.

The tumor sections of the mice treated with USPIO/SQgem NPs without exposure to magnetic field revealed a negligible presence of the iron content as indicated by faible staining. On the contrary, the tumor sections of the mice treated with the magnetically-guided USPIO/SQgem NPs showed significant accumulation of iron, mainly deposited at the tumor periphery, where the external magnet was placed (see supporting Figure 13). This is explainable by the fact that the tumors were isolated immediately after removing the external magnetic field. In these conditions, the particles were not provided with enough time to diffuse into the tumor interstitium. However, it is expected that after the USPIO/SQgem NPs at the tumor periphery are relieved from the influence of the extracorporeal magnetic field, they will likely diffuse into the tumor matrix and elicit the therapeutic response as evidenced by the impressive anticancer efficacy as seen in Figure 3.

2.14. Characterization of $SQGd^{3+}$ micelles and SQgem/$SQGd^{3+}$ composite nanoparticles

2.14.1. Geometry and surface electrical properties

Geometry (size and shape) and electrophoretic characterizations (Table S1) were performed as previously described (see supporting sections 2.11.1., and 2.11.3.). The

SQgem NPs and SQgem/SQGd^{3+} composite NPs, previously incubated with glycerol (30 %, v/v), used as a cryoprotectant, were visualised by transmission electron microscopy after freeze-fracture (FF-TEM). For this, a drop of each sample was placed on a copper support and immediately frozen in liquid propane, surrounded by liquid nitrogen, and then kept in liquid nitrogen. Fracturing and shadowing were performed in a BAL-TEC BAF 060 - Freeze Fracture & Freeze Etch System (Liechtenstein). The replicas were washed in THF and distilled water, and placed on copper grids.

2.14.2. Small-angle X-ray scattering (SAXS)

The structure of the SQgem/SQGd^{3+} composite NPs was further investigated by small-angle X-ray scattering (SAXS). Experiments were performed on the SWING synchrotron beamline at Synchrotron SOLEIL,[31] operated at 12 keV. Sample was loaded in a quartz capillary (1.5 mm diameter, GLASS W. Müller, Berlin, Germany). X-ray pattern was recorded at 20.0 ± 0.5 ºC by a two-dimensional CCD detector. The scattered intensity is reported as a function of the scattering vector:

$$q = \frac{4\pi \sin(\theta)}{\lambda} \tag{8}$$

where 2θ is the scattering angle, and λ the wavelength. From this scattering vector, it is possible to calculate the distances (d) as follows:

$$q = \frac{2\pi}{d} \tag{9}$$

The calibration of the q-range was carried out with the 2Lβ form of pure tristearin (d-spacing: 44.97 ± 0.05 Å), and silver behenate (d-spacing: 58.38 ± 0.01 Å). In order to

determine the peak positions, diffractograms were fitted with the Gaussian model by the use of IGOR pro-software (WaveMetrics, Inc., USA).

The cubic structure of the SQgem/SQGd^{3+} nanocomposites was identified by SAXS (Figure S14). The curve was compatible with a cubic phase *Pn3m*, where the series has an onset at scattering vector q = 0.086, and the obtained experimental values of the lattice were 0.086, 0.1034, 0.144, and 0.166, whereas the calculated values of the cubic phase *Pn3m*: 0.086, 0.1053, 0.1216, 0.149, and 0.172. Hence, q values spaced in the ratios √2, √3, 2, √6, √8, and 3. These peaks indexed as the (110), (111), (200), (211), (220), and (221) reflections of a cubic lattice of space group *Pn3m*.[32] The organization of the nanocomposites into a cubic phase was clearly different from that of SQgem NPs alone, which were organized into a hexagonal inverse phase.[5] A particularly attractive feature is that SQgem/SQGd^{3+} spontaneously formed NPs with reproducible mean size, without the need of high-energy dispersing methods or dispersing agents, unlike in many other systems.[33]

2.14.3. Determination of the amount of SQGd^{3+} in the SQgem/SQGd^{3+} nanocomposites

Freshly prepared aqueous suspensions of SQgem/SQGd^{3+} NPs were centrifuged at 20.0 ± 0.5 °C in an Optima LE-80K ultracentrifuge (Beckman Coulter, USA; 70.1 Ti rotor) at 40.000 rpm for 60 min. Supernatants were collected to remove the non-entrapped SQGd^{3+} complex. The amount of SQGd^{3+} entrapped into the SQgem/SQGd^{3+} nanocomposites was determined as the difference between the total amount of SQGd^{3+} used in the preparation of the nanocomposites and the amount of SQGd^{3+} detected in the

supernatant. The entrapment yield was calculated as the ratio between the amount of entrapped $SQGd^{3+}$ and the total amount of $SQGd^{3+}$ added in the preparation procedure.

Practically, the amount of $SQGd^{3+}$ in the supernatant was determined by the Evans' method.[8,9] Briefly, 25 μL of tert-butanol were added as standard to 500 μL of supernatant. ^{1}H-nuclear magnetic resonance (^{1}H-NMR) spectra were acquired (Bruker Avance-400, USA; 400 MHz, 298 K) in the presence of an inner insert cell containing an internal standard [100 μL of deuterium oxide (D_2O) and 25 μL of tert-butanol]. By measuring the difference of the chemical shift ($\Delta\delta$, ppm) between the signals of tert-butanol from the two solutions, it was possible to calculate the exact amount of paramagnetic agent present in the supernatant solution using the following equation:

$$\Delta\delta = \frac{4000\pi cs}{T} \times \left(\frac{\mu_{eff}}{2.84} \right)^2 \qquad (10)$$

in which c is the concentration of the $SQGd^{3+}$, s = 1/3 (for cryomagnet), T is the absolute temperature (ºK), and μ_{eff} is the magnetic moment of the lanthanide metal (7.94 for Gd^{3+}).

The entrapment yield of $SQGd^{3+}$ into SQgem was 46 ± 6 wt %.

2.14.4. Proton nuclear magnetic relaxation rate analysis

^{1}H-nuclear magnetic relaxation dispersion (^{1}H-NMRD) profiles were obtained at 310 ºK on a field cycling relaxometer (Stelar, Italy). The range of magnetic fields covered varied from 0.47 mT to 0.24 T, which corresponds to frequencies ranging from 0.02 to 10 MHz. Additional longitudinal and transverse relaxation rates were measured on Bruker Minispecs mq20 and mq60 (Bruker, Germany) at 20 MHz (0.47 T) and 60 MHz (1.41 T), respectively. T_1 relaxation times were recorded at 37.0 ± 0.5 ºC for $SQGd^{3+}$ and

SQgem/SQGd^{3+} in the concentration ranges 0.1 – 2mM of Gd^{3+} derivative. The T_1 relaxivity (r_1) of the SQGd^{3+} complex was determined as follows:

$$r_1 = \frac{R_1^{obs} - R_1^{m}}{C} \quad (11)$$

where R_1^{obs} and R_1^{m} are the relaxation rates (s^{-1}) of the sample and suspension media (water), respectively; and C is the concentration of the paramagnetic SQGd^{3+} (mM). The relaxivity measurements (Table S1) were performed on samples at concentrations higher than the CMC. Under these conditions, the contribution of the monomeric species is negligible, and aggregates are mostly responsible for the measured relaxivity values.[34]

Remarkably, very high relaxivity values were found in the case of SQGd^{3+} (≈ 22 $mM^{-1}\cdot s^{-1}$). These values are among the highest ones reported in the literature.[43,35] Noticeably, other Gd^{3+} complexes coupled to lipophilic groups such as cholesterol (Chol) were unable to associate in water and thus their relaxivities were much lower (4.42 $mM^{-1}\cdot s^{-1}$, at 25.0 ± 0.5 °C and 20 MHz), *i.e.* in the same order of magnitude as the clinically used Dotarem® (5.25 $mM^{-1}\cdot s^{-1}$).[36]

A slight decrease in relaxivity was found in the case of SQgem/SQGd^{3+} NPs (≈ 20 $mM^{-1}\cdot s^{-1}$), compared to the SQGd^{3+} micelles (≈ 22 $mM^{-1}\cdot s^{-1}$) (Table S1). This could be the consequence of the different water accessibilities of Gd^{3+} ions into the SQGd^{3+} micelles, compared to the SQgem/SQGd^{3+} NPs.

The measurement of ^{1}H-NMRD profiles over an extended range of magnetic field strengths (0.01 – 60 MHz) is a complementary method for the complete characterization of a paramagnetic complex. The ^{1}H-NMRD profile (r_1 *vs.* proton Larmor frequency) for SQGd^{3+} (Figure S15) shows that this complex possesses high relaxivity values at all fields, with a marked peak centred at 30 MHz. The ^{1}H-NMRD profiles of the micelles are

characteristic of slowly tumbling molecules, caused by an increase in the rotational correlation time (τ_R) with the typical high-field peak around 20 – 30 MHz.[35] These values are similar to those reported for other Gd^{3+} complex bound to macromolecules.[8,9]

2.15. Statistical analysis

Statistical analysis was performed using Student's *t*-test. Data with $p < 0.05$ and $p < 0.001$ were considered as significant and very significant, respectively.

SUPPORTING REFERENCES

1. Massart, R. Preparation of Aqueous Magnetic Liquids in Alkaline and Acidic Media. *IEEE Trans. Magn.* **1981**, *17***,** 1247–1248.
2. Couvreur, P.; Stella, B.; Reddy, L. H.; Hillaireau, H.; Dubernet, C.; Desmaële, D.; Lepêtre-Mouelhi, S.; Rocco, F.; Dereuddre-Bosquet, N.; Clayette, P.; *et al*. Squalenoyl Nanomedicines as Potential Therapeutics. *Nano Lett.* **2006**, *6*, 2544–2548.
3. Caravan, P.; Ellison, J. J.; McMurry, T. J.; Lauffer. R. B. Gadolinium(III) Chelates as MRI Contrast Agents: Structure, Dynamics, and Applications. *Chem. Rev.* **1999**, *99***,** 2293–2352.
4. Semmler, W.; Schwaiger, M. *Handbook of Experimental Pharmacology*, Vol. 185, Springer-Verlag: Berlin Heidelberg, 2008.
5. Couvreur, P.; Reddy, L. H.; Mangenot, S.; Poupaert, J. H.; Desmaële, D.; Lepêtre-Mouelhi, S.; Pili, B.; Bourgaux, C.; Amenitsch, H.; Ollivon, M. Discovery of New Hexagonal Supramolecular Nanostructures Formed by Squalenoylation of an Anticancer Nucleoside Analogue. *Small* **2008**, *4***,** 247–253.
6. Bekkara-Aounallah, F.; Gref, R.; Othman, M.; Reddy, L. H.; Pili, B.; Allain, V.; Bourgaux, C.; Hillaireau, H.; Lepêtre-Mouelhi, S.; Desmaële, D.; *et al*. Novel PEGylated Nanoassemblies Made of Self-Assembled Squalenoyl Nucleoside Analogues. *Adv. Funct. Mater.* **2008**, *18***,** 1–11.
7. Barge, A.; Cravotto, G.; Gianolio, E.; Fedeli, F. How to Determine Free Gd and Free Ligand in Solution of Gd Chelates. A Technical Note. *Contrast Med. Mol. Imaging* **2006**, *1***,** 184–188.

8. Corsi, D. M.; Platas-Iglesias, C.; van Bekkum, H.; Peters, J. A. Determination of Paramagnetic Lanthanide (III) Concentrations from Bulk Magnetic Susceptibility Shifts in NMR Spectra. *Magn. Reson. Chem.* **2001**, *39***,** 723–726.
9. Battistini, E.; Gianolio, E.; Gref, R.; Couvreur, P.; Fuzerova, S.; Othman, M.; Aime, S.; Badet, B.; Durand, P. High-Relaxivity Magnetic Resonance Imaging (MRI) Contrast Agent based on Supramolecular Assembly between a Gadolinium Chelate, a Modified Dextran, and Poly-β-cyclodextrin. *Chemistry* **2008**, *14***,** 4551–4561.
10. Gløgård, C.; Hovland, R.; Fossheim, S. L.; Aasen, A. J.; Klaveness, J. Synthesis and Physicochemical Characterisation of New Amphiphilic Gadolinium DO3A Complexes as Contrast Agents for MRI. *J. Chem. Soc*. *Perkin Trans.* **2000**, *2***,** 1047–1052.
11. Francis, M. F.; Lavoie, L.; Winnik, F. M.; Leroux, J. C. Solubilization of Poorly Water Soluble Drugs in Micelles of Hydrophobically Modified Hydroxypropylcellulose Copolymers. *Eur. J. Pharm. Biopharm.* **2003**, *56***,** 337–346.
12. Wilhelm, M.; Zhao, C. L.; Wang, Y.; Xu, R.; Winnik, M. A.; Mura, J. L.; Riess, G.; Croucher, M. D. Poly(styrene-ethylene oxide) Block Copolymer Micelle Formation in Water: a Fluorescence Probe Study. *Macromolecules* **1991**, *24***,** 1033–1040.
13. Arias, J. L.; Reddy, L. H.; Couvreur, P. Polymeric Nanoparticulate System Augmented the Anticancer Therapeutic Efficacy of Gemcitabine. *J. Drug Target.* **2009**, *17***,** 586–598.
14. Moog, R.; Burger, A. M.; Brandl, M.; Schüler, J.; Schubert, R.; Unger, C.; Fiebig, H. H.; Massing, U. Change in Pharmacokinetic and Pharmacodynamic Behavior of

Gemcitabine in Human Tumor Xenografts upon Entrapment in Vesicular Phospholipid Gels. *Cancer Chemother. Pharmacol.* **2002**, *49***,** 356–366.

15. Yang, J.; Park, S. B.; Yoon, H. G.; Huh, Y. M.; Haam, S. Preparation of Poly Epsilon-caprolactone Nanoparticles Containing Magnetite for Magnetic Drug Carrier. *Int. J. Pharm.* **2006**, *324***,** 185–190.
16. Tardi, P.; Boman, N.; Cullis, P. Liposomal Doxorubicin. *J. Drug Target.* **1996**, *4***,** 129–140.
17. Yoo, H. S.; Park, T. G. Biodegradable Polymeric Micelles Composed of Doxorubicin Conjugated PLGA-PEG Block Copolymer. *J. Control. Release* **2001**, *70***,** 63–70.
18. Straubinger, R. M.; Balasubramanian, S. V. Preparation and Characterization of Taxane-Containing Liposomes. *Methods Enzymol.* **2005**, *391***,** 97–117.
19. Zhang, Z.; Feng, S. S. Self-Assembled Nanoparticles of Poly(lactide)--Vitamin E TPGS Copolymers for Oral Chemotherapy. *Int. J. Pharm.* **2006**, *324*, 191–198.
20. Woo, J.; Chiu, G. N.; Karlsson, G.; Wasan, E.; Ickenstein, L.; Edwards, K.; Bally, M. B. Use of a Passive Equilibration Methodology to Encapsulate Cisplatin into Preformed Thermosensitive Liposomes. *Int. J. Pharm.* **2008**, *349*, 38–46.
21. Avgoustakis, K.; Beletsi, A.; Panagi, Z.; Klepetsanis, P.; Karydas, A. G.; Ithakissios, D. S. PLGA-mPEG Nanoparticles of Cisplatin: in Vitro Nanoparticle Degradation, in Vitro Drug Release and in Vivo Drug Residence in Blood Properties. *J. Control. Release* **2002**, *79***,** 123–135.
22. O'Brien, R. W.; White, L. R. Electrophoretic Mobility of a Spherical Colloidal Particle. *J. Chem. Soc. Faraday Trans.* **1978**, *2***,** 1607–1626.

23. Plaza, R. C.; Arias, J. L.; Espín, M.; Jiménez, M. L.; Delgado, A. V. Aging Effects in the Electrokinetics of Colloidal Iron Oxides *J. Colloid Interface Sci.* **2002**, *245*, 86–90.

24. Lyklema, J. The Role of Surface Conduction in the Development of Electrokinetics. In *Interfacial Electrokinetics and Electrophoresis*; Delgado, A.V., Ed.; Marcel Dekker: New York, 2002, 87–98.

25. van Oss, C. J. *Interfacial Forces in Aqueous Media*, ed. 2, CRC Press: Boca Raton, 2006.

26. Plaza, R. C.; Zurita, L.; Durán, J. D. G.; González-Caballero, F.; Delgado, A. V. Surface Thermodynamics of Hematite/Ytrium Oxide Core-Shell Colloidal Particles. *Langmuir* **1998**, *14*, 6850–6854.

27. Arias, J. L.; Gallardo, V.; Gómez-Lopera, S. A.; Plaza, R.; Delgado, A. V. Synthesis and Characterization of Poly(ethyl-2-cyanoacrylate) Nanoparticles with a Magnetic Core. *J. Control. Release* **2001**, *77*, 309–321.

28. López-López, M. T.; Durán, J. D. G.; Delgado, A. V.; González-Caballero, F. Stability and Magnetic Characterization of Oleate-Covered Magnetite Ferrofluids in Different Nonpolar Carriers. *J. Colloid Interface Sci.* **2005**, *291*, 144–151.

29. Scholzen, T.; Gerdes, J. The Ki-67 Protein: From the Known and the Unknown. *J. Cell Physiol.* **2000**, *182*, 311–322.

30. Gang, J.; Park, S. B.; Hyung, W.; Choi, E. H.; Wen, J.; Kim, H. S., Shul, Y. G.; Haam, S.; Song, S. Y. Magnetic Poly ε-Caprolactone Nanoparticles Containing Fe_3O_4 and Gemcitabine Enhance Anti-Tumor Effect in Pancreatic Cancer Xenograft Mouse Model. *J. Drug Target.* **2007**, *15*, 445–453.

31. Official website of Synchrotron SOLEIL (http://www.synchrotron-soleil.fr/Recherche/LignesLumiere/SWING).
32. Seddon, J. M.; Robins, J.; Gulik-Krzywicki, T.; Delacroix, H. Inverse Micellar Phases of Phospholipids and Glycolipids. *Phys. Chem. Chem. Phys.* **2000**, *2*, 4485–4493.
33. Almgren, M.; Rangelov, S. J. Polymorph Dispersed Particles from the Bicontinuous Cubic Phase of Glycerol Monooleate Stabilized by PEG-Copolymers with Lipid-Mimetic Hydrophobic Anchors. *J. Dispersion Sci. Technol.* **2006**, *27*, 599–609.
34. Accardo, A.; Tesauro, D.; Aloj, L.; Pedone, C.; Morelli, G. Supramolecular Aggregates Containing Lipophilic Gd(III) Complexes as Contrast Agents in MRI. *Coord. Chem. Rev.* **2009**, *253*, 2193–2213.
35. Nicolle, G. M.; Tóth, É.; Eisenwiener, K. P.; Mäcke, H. R.; Merbach, A. E. From Monomers to Micelles: Investigation of the Parameters Influencing Proton Relaxivity. *J. Biol. Inorg. Chem.* **2002**, *7*, 757–769.
36. Oliver, M.; Ahmad, A.; Kamaly, N.; Perouzel, E.; Caussin, A.; Keller, M.; Herlihy, A.; Bell, J.; Miller, A. D.; Jorgensen, M. R. MAGfect: A Novel Liposome Formulation for MRI Labelling and Visualization of Cells. *Org. Biomol. Chem.* **2006**, *4*, 3489–3497.

SUPPORTING FIGURES

Supporting Figure 1. High resolution transmission electron microscopy picture of USPIO particles. Bar length: 10 nm.

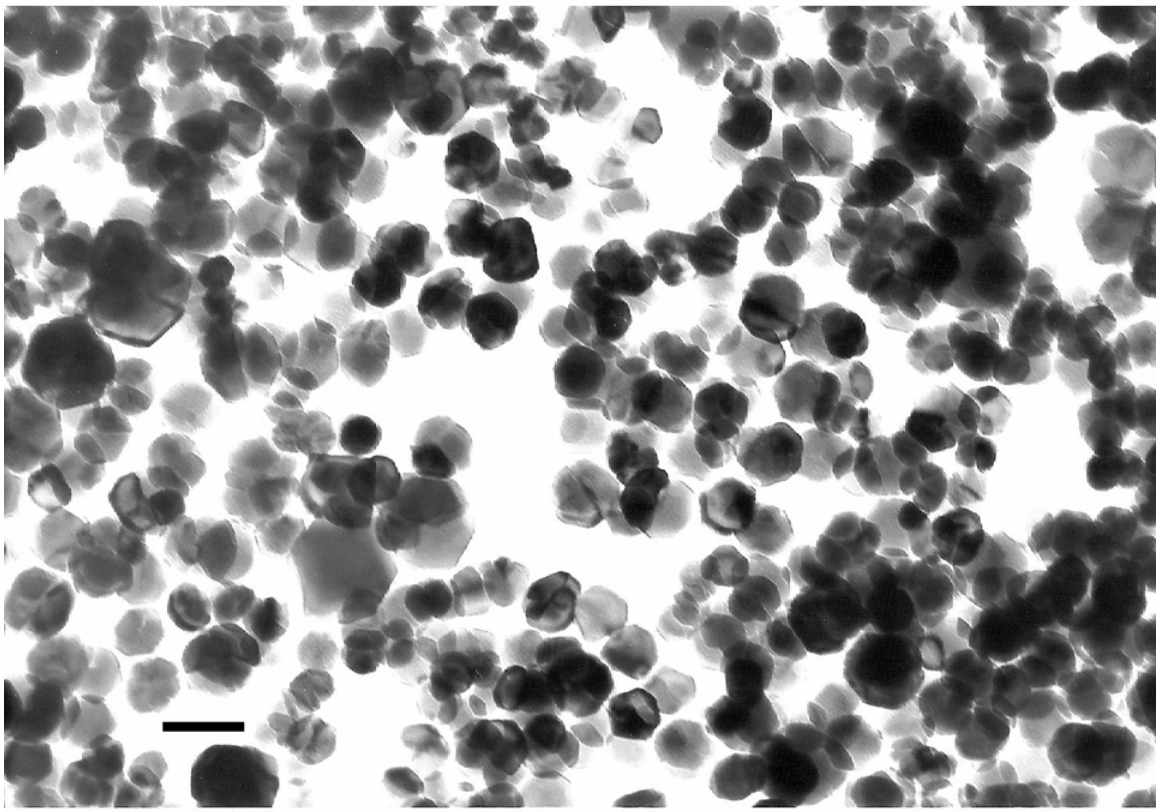

Supporting Figure 2a. Synthesis of the squalenoyl gemcitabine (SQgem) (**3**). Reagents and conditions: (i) EtOCOCl, Et_3N, THF, 0 °C, and 30 min. (ii) Gemcitabine·HCl, Et_3N, DMF, 20 °C, and 72 h.

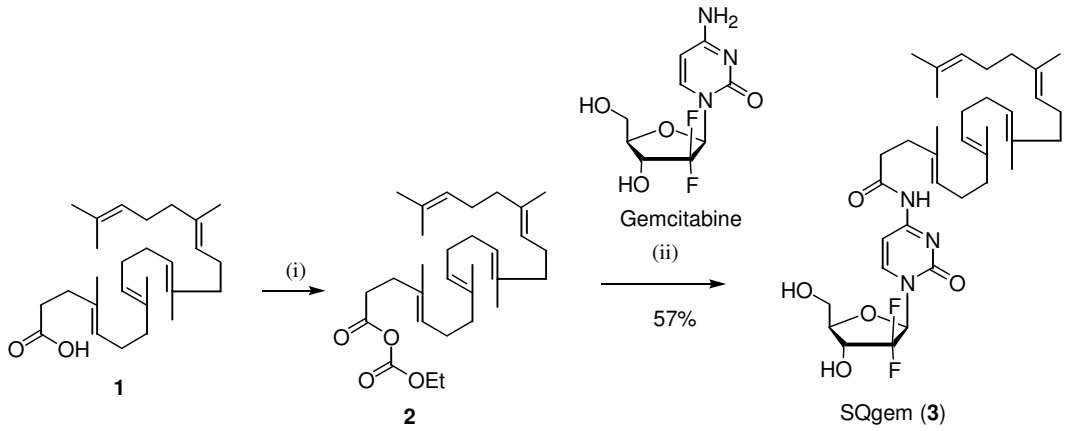

Supporting Figure 2b. Synthesis of the squalenoyl doxorubicin (SQdox) (**6**). Reagents and conditions: (i) $(MeO)_3CH$, Br_2, acetone, 30 °C, 40 min. (ii) 1) (**1**), K_2CO_3, acetone, 20 °C, 20 h; 2) HCl, Et_2O.

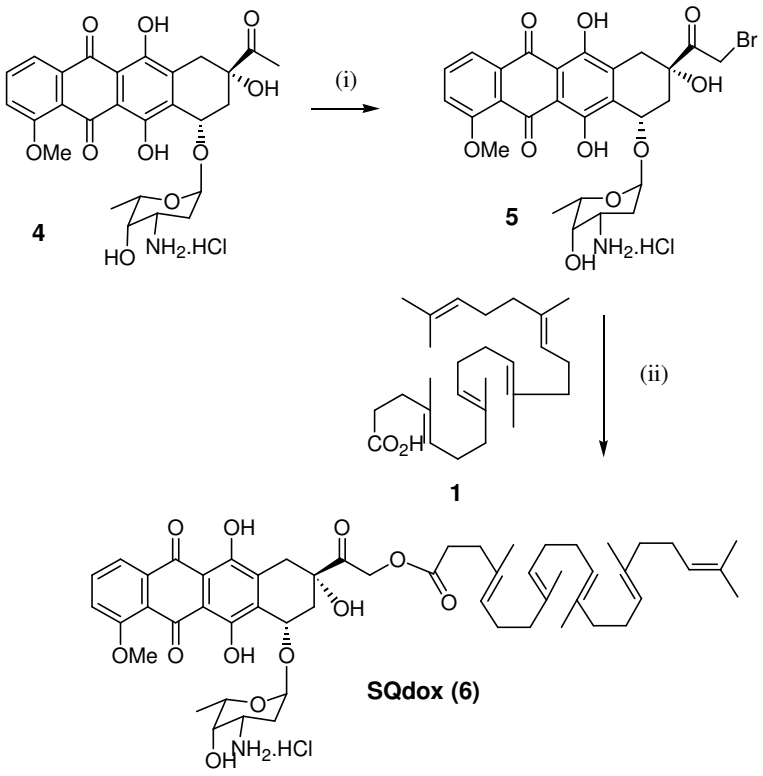

Supporting Figure 2c. Synthesis of the squalenoyl paclitaxel (SQptx) (**8**). Reagents and conditions: (i) EDAC, DMAP, dichloromethane, 20 °C.

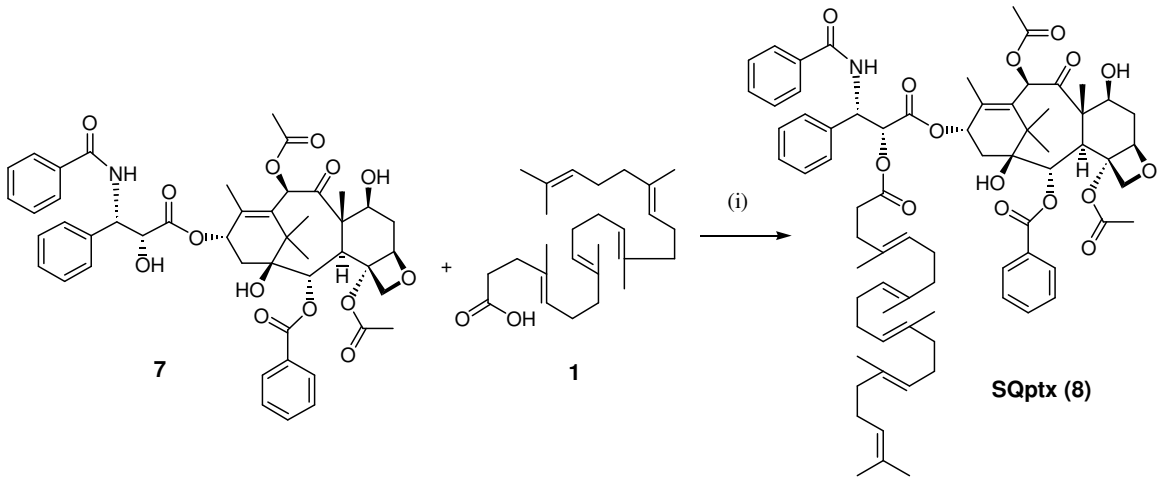

Supporting Figure 2d. Synthesis of the squalenoyl cisplatin (SQcis) (**12**). Reagents and conditions: (i) 30 % H_2O_2, 50 °C, 1 h 30 min. (ii) succinic anhydride, DMF, 70 °C, 6 h. (iii) 1) EtOCOCl, Et_3N, THF, DMF, 0 °C, 30 min; 2) tris-nor-squalenamine (**11**), DMF, 20 °C, 4d.

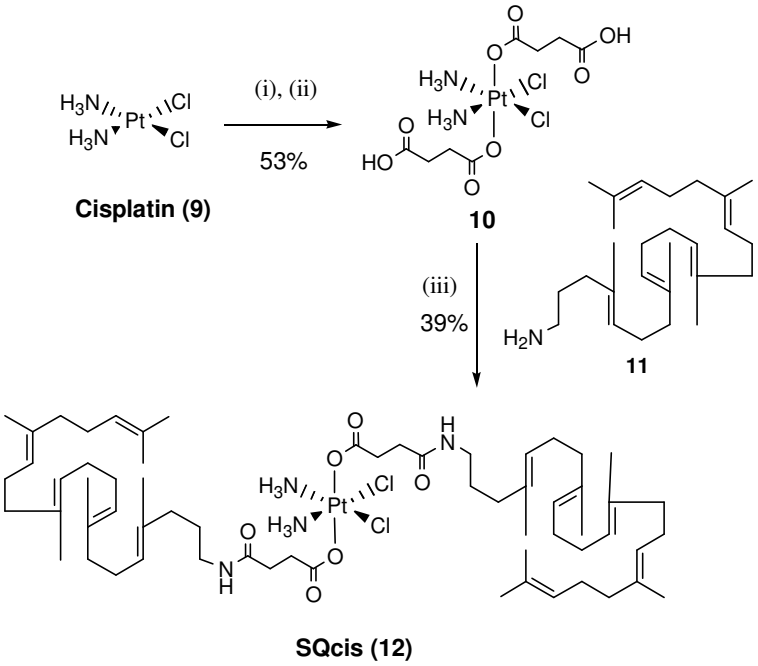

Supporting Figure 2e. Synthesis of the squalenoyl-DOTA Gd^{3+} complex ($SQGd^{3+}$) (**20**). Reagents and conditions: (i) 1) EtOCOCl, Et_3N, acetone, 0 °C; 2) NaN_3, H_2O. (ii) EtOH, toluene 110 °C. (iii) KOH 1N, EtOH, 80 °C. (iv) $BrCH_2CO_2H$, EDCI·HCl, DMAP, LiBr, CH_2Cl_2; (v) DO3AEt (**17**), K_2CO_3, CH_3CN. (vi) $LiOH·H_2O$, MeOH, THF, H_2O. (vii) $GdCl_3·6H_2O/H_2O$.

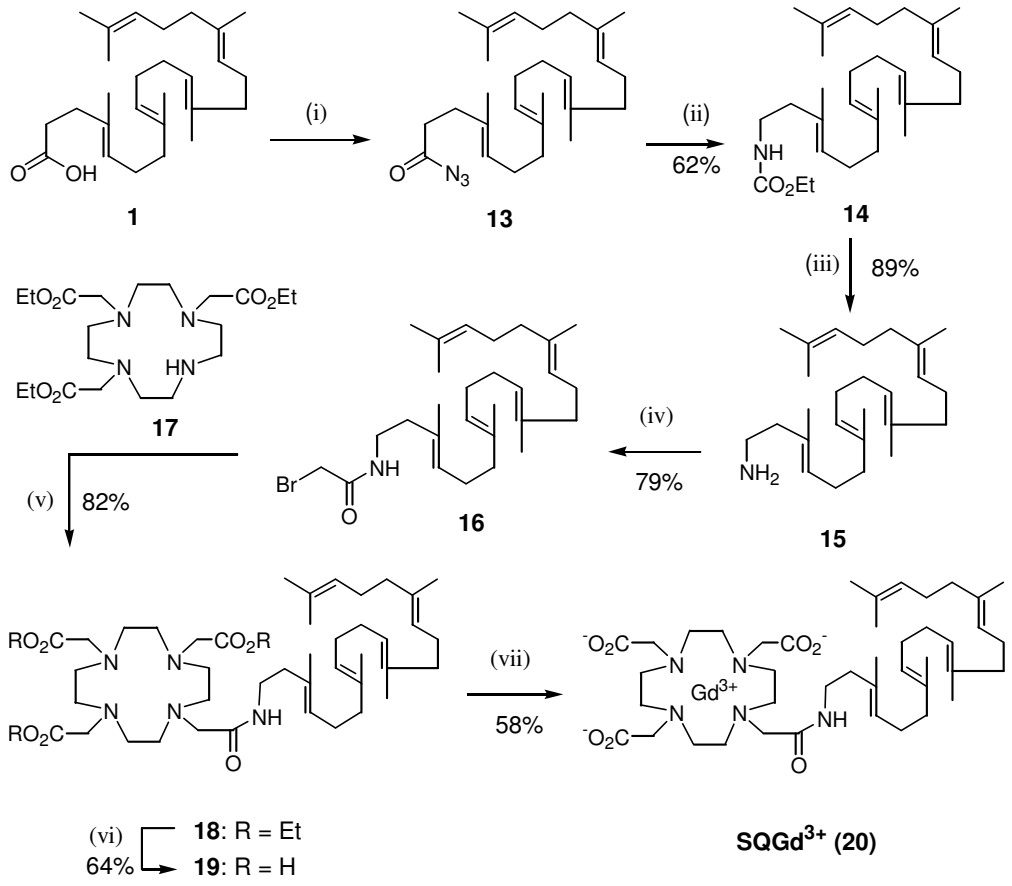

Supporting Figure 3. ESI$^+$ mass spectrum of SQGd^{3+} complex (**20**), located around m/z = 919.7 [M+LiH]$^+$, 935.7 [M+Na]$^+$, and 951.6 [M+K]$^+$, showing the characteristic isotopic pattern of Gd^{3+}.

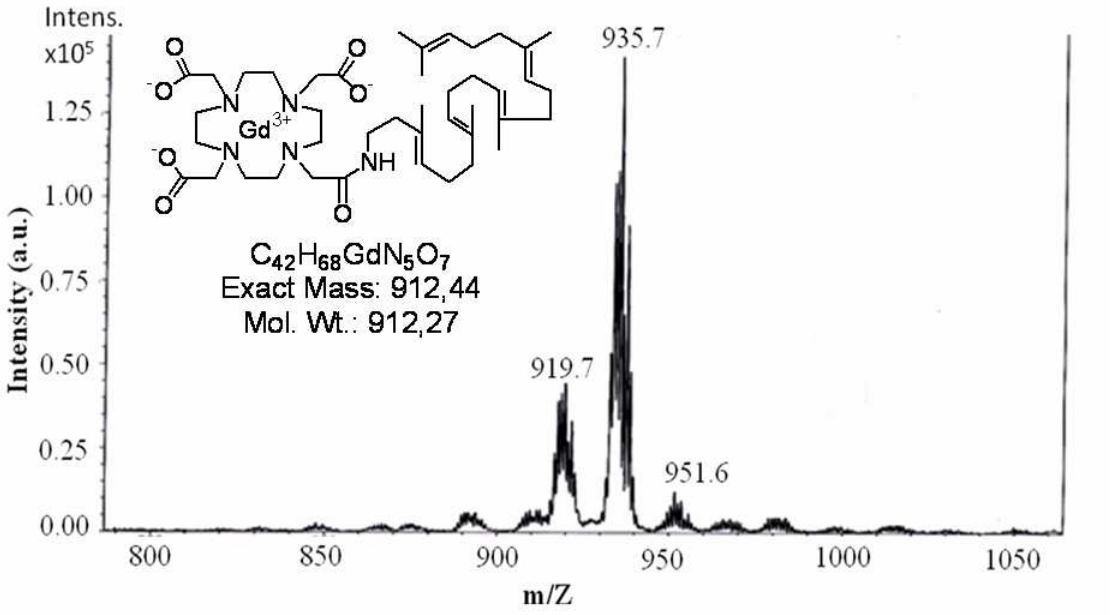

Supporting Figure 4. Experimental determination of the CMC of $SQGd^{3+}$ by monitoring the changes in the I_{336}/I_{333} ratio of pyrene fluorescence intensity as a function of the logarithm of $SQGd^{3+}$ concentration ($1 - 5 \times 10^3$ mg/L).

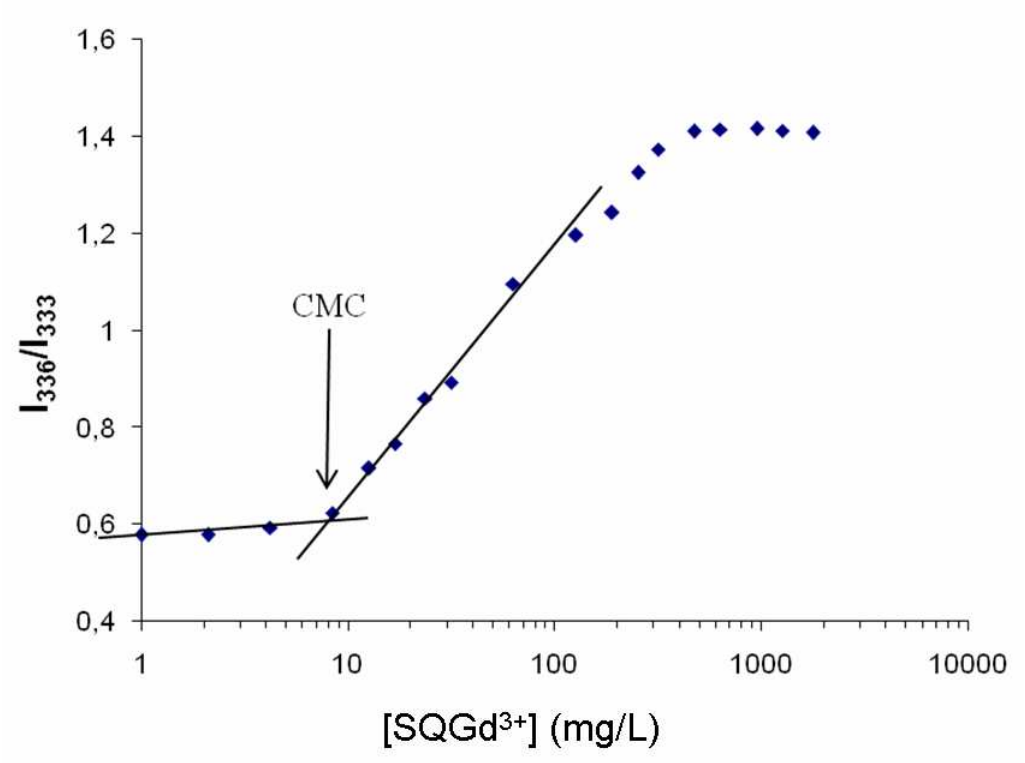

Supporting Figure 5. Zeta potential (ζ) of nanomagnetite (■, USPIO), squalenoyl antitumor prodrug NPs (●, SQgem, SQdox, SQptx, SQcis), and nanomagnetite/squalenoyl antitumor prodrug composite NPs (○, USPIO/SQgem, USPIO/SQdox, USPIO/SQptx, USPIO/SQcis) as a function of pH in the presence of 10^{-3} M NaCl. The lines are a guide to the eye. USPIO showed a well-defined isoelectric point (pH_{iep} or pH of zero potential) in the vicinity of pH = 7 corresponding to the amphoteric thin oxide layer.[23] Such behaviour cannot be found with SQgem (pH_{iep} was ≈ 4.2) and USPIO/SQgem NPs which also displayed a neutral charge ≈ pH 4.5 (Figure S5a). Additionaly, the other pure squalenoyl antitumor prodrug NPs and their corresponding magnetic nanocomposites [USPIO/SQdox (Figure S5b), USPIO/SQptx (Figure S5c), and USPIO/SQcis (Figure S5d)] have a negative surface charge for the whole pH range studied and only at pH < 4, the zeta potential can approach a zero value. Depending on the structure of the squalenoyl composite materials, the generation of a surface charge is likely due to the ester bonds (which could be hydrolyzed, resulting in carboxylic functions that may account for the observed ζ negative values), and/or weak alcoholic of SQgem, SQdox, SQptx, and SQcis. In addition, pluronic® F-68 hydroxyl moieties which remained adsorbed onto the surface, even after the cleaning procedure, may also slightly account for the pH dependency of the surface charge.

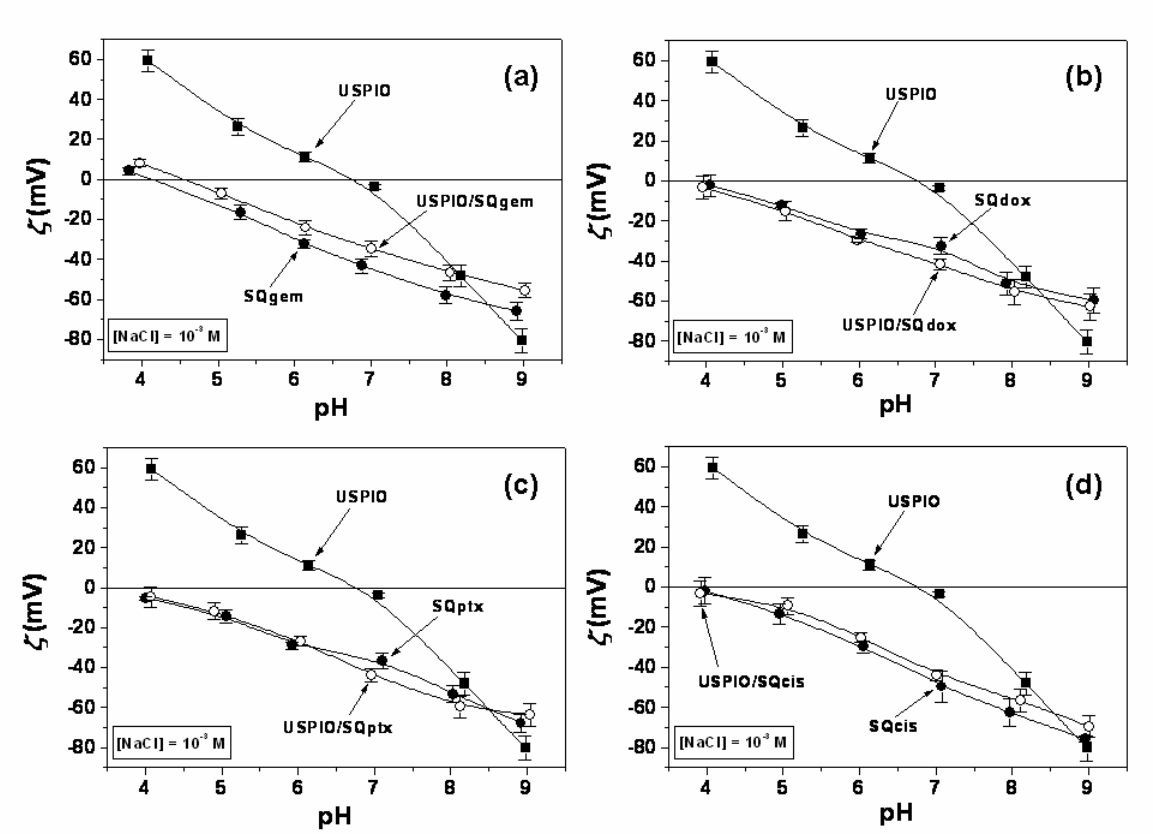
(a)
USPIO
USPIO/SQgem
SQgem
[NaCl] = 10⁻³ M
ζ (mV)
pH
(b)
USPIO
SQdox
USPIO/SQdox
[NaCl] = 10⁻³ M
ζ (mV)
pH
(c)
USPIO
SQptx
USPIO/SQptx
[NaCl] = 10⁻³ M
ζ (mV)
pH
(d)
USPIO
USPIO/SQcis
SQcis
[NaCl] = 10⁻³ M
ζ (mV)
pH

Supporting Figure 6. Zeta potential (ζ) of nanomagnetite (■, USPIO), squalenoyl antitumor prodrug NPs (●, SQgem, SQdox, SQptx, SQcis), and nanomagnetite/squalenoyl antitumor prodrug composite NPs (○, USPIO/SQgem, USPIO/SQdox, USPIO/SQptx, USPIO/SQcis) as a function of the NaCl concentration at pH = 5.6. The lines are a guide to the eye. The absolute value of ζ changed differently with the ionic strength depending on the type of material: in the case of pure squalenoyl antitumor prodrug NPs and their corresponding magnetic nanocomposites [USPIO/SQgem (Figure S6a), USPIO/SQdox (Figure S6b), USPIO/SQptx (Figure S6c), and USPIO/SQcis (Figure S6d)], a decrease in $|\zeta|$ was observed when the electrolyte concentration was increased, due to the classical double-layer compression mechanism. However, USPIO displayed a different trend: $|\zeta|$ slightly went through a maximum ($\approx 10^{-3}$ M NaCl), so that the compression was slightly observed only at high enough electrolyte concentration. This slight initial increase of $|\zeta|$ with concentration could be a consequence of the manifestation of stagnant-layer conductivity,[24] which became less significant when the diffuse layer was richer in counterions (this occurs if the bulk concentration of ions is large enough). Hence, the classical behaviour was slightly recovered at the high NaCl concentrations used in this study.

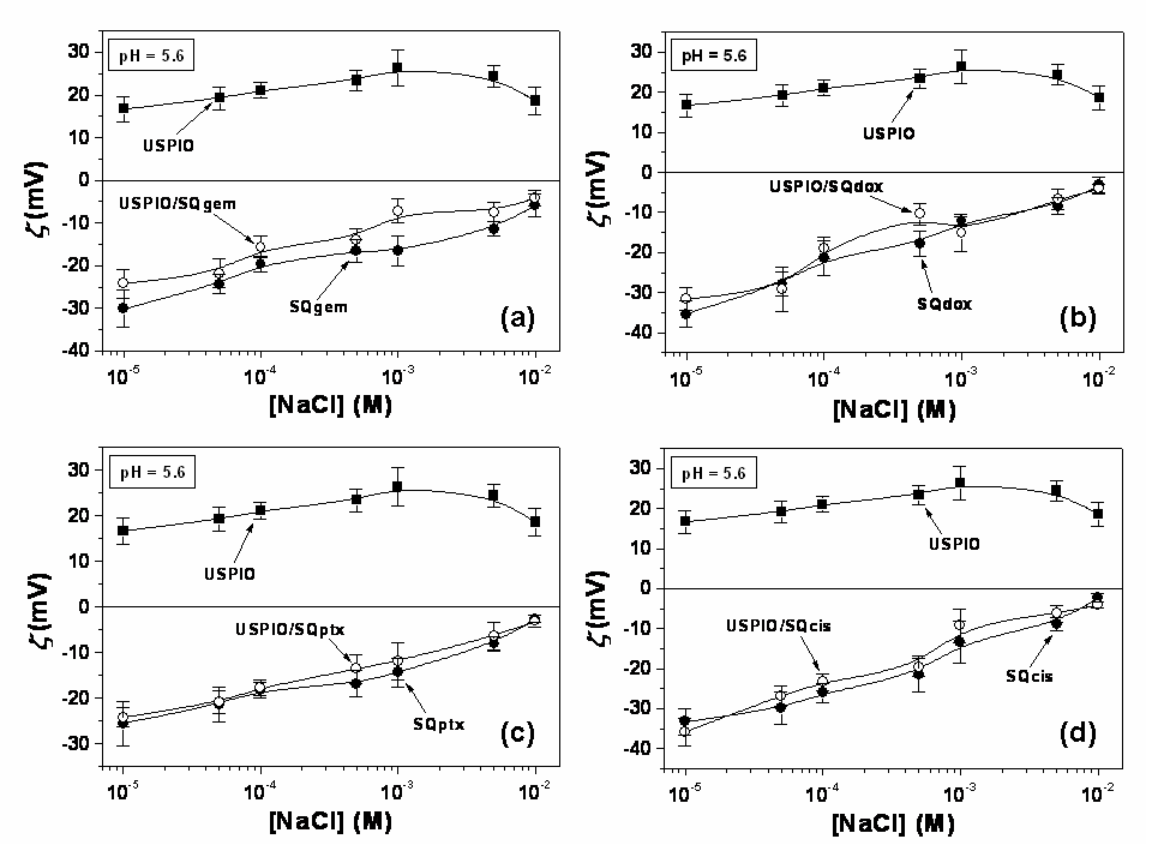
pH = 5.6
USPIO
USPIO/SQgem
SQgem
(a)
ζ (mV)
[NaCl] (M)
pH = 5.6
USPIO
USPIO/SQdox
SQdox
(b)
ζ (mV)
[NaCl] (M)
pH = 5.6
USPIO
USPIO/SQptx
SQptx
(c)
ζ (mV)
[NaCl] (M)
pH = 5.6
USPIO
USPIO/SQcis
SQcis
(d)
ζ (mV)
[NaCl] (M)

Supporting Figure 7. (a) Contact angle θ (degrees) of the probe liquids on USPIO, squalenoyl antitumor prodrugs (SQgem, SQdox, SQptx, and SQcis), and USPIO/squalenoyl antitumor prodrug composites (USPIO/SQgem, USPIO/SQdox, USPIO/SQptx, and USPIO/SQcis), and (b) corresponding surface free energy components (mJ/m^2) of these materials. γ_S^{LW} is the Lifshitz-van der Waals component; γ_S^+ (γ_S^-) is the electron-acceptor (electron-donor) component. Whatever the component considered, its values for the magnetic composites were similar to those obtained for the pure squalenoyl prodrugs (γ_S^+ is not suitable for the comparison, as it displayed values close to zero in all the materials). Although γ_S^{LW} was the least affected, its value for the magnetic composites was almost the same as that of the pure squalenoyl prodrug NPs. However, the electron-donor component (γ_S^-) is the quantity that seemed the most sensitive to the surface composition. The USPIO γ_S^- component was important, as in many other inorganic oxides (*e.g.*, hematite and yttria),[26] showing that it is a monopolar, electron-donor material. Due to their almost non-polar character, pure squalenoyl prodrugs gave rise to a measurable decrease in the γ_S^- of magnetic nanocomposites as compared to USPIO.

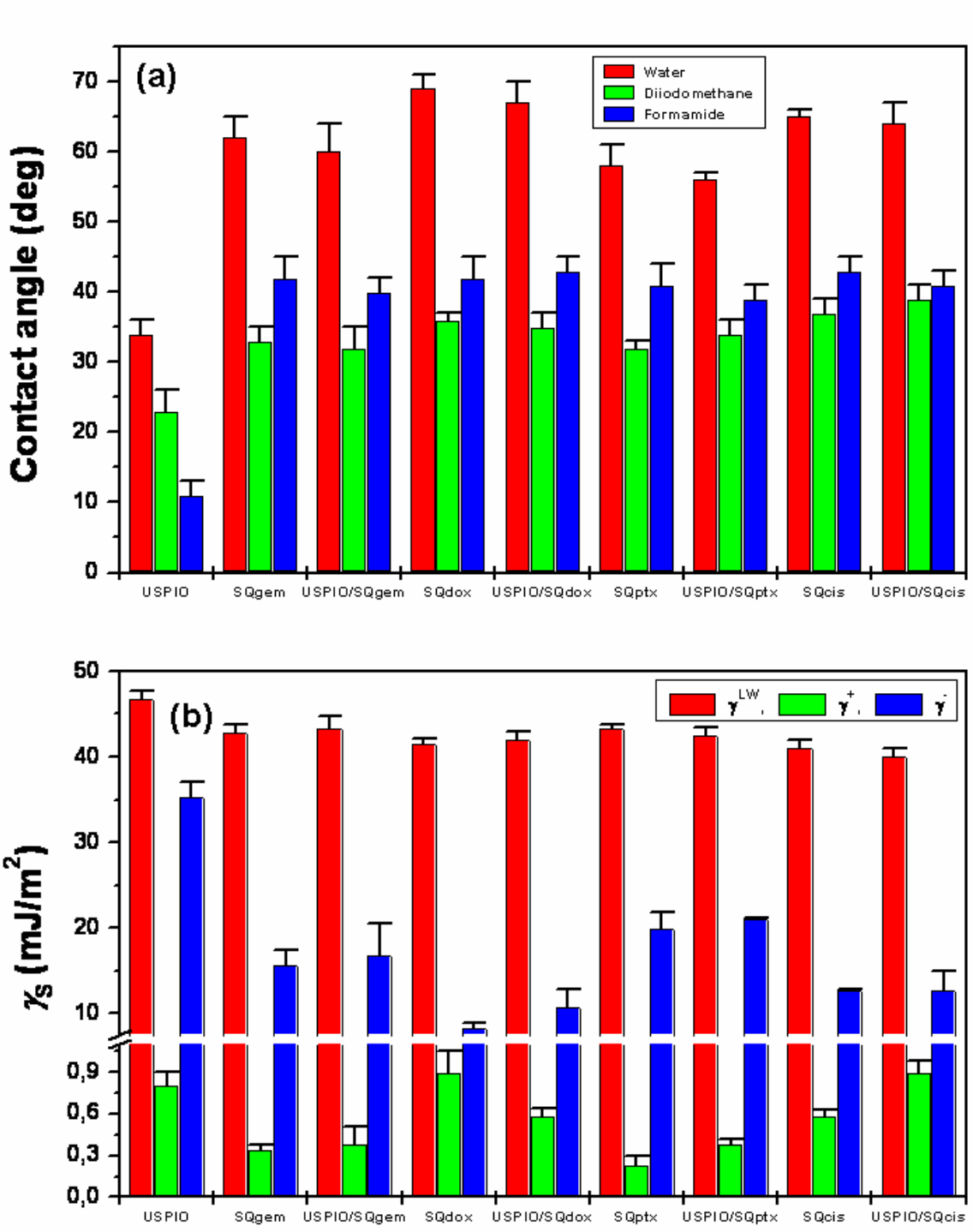
(a)
Water
Diiodomethane
Formamide
Contact angle (deg)
0
10
20
30
40
50
60
70
USPIO
SQgem
USPIO/SQgem
SQdox
USPIO/SQdox
SQptx
USPIO/SQptx
SQcis
USPIO/SQcis
(b)
γ_s^{LW}
γ_s^{+}
γ_s^{-}
γ_s (mJ/m^2)
0,0
0,3
0,6
0,9
10
20
30
40
50
USPIO
SQgem
USPIO/SQgem
SQdox
USPIO/SQdox
SQptx
USPIO/SQptx
SQcis
USPIO/SQcis

Supporting Figure 8. ΔG_{SLS} values and hydrophobicity/hydrophilicity of USPIO, squalenoyl antitumor prodrugs (SQgem, SQdox, SQptx, and SQcis), and USPIO/squalenoyl antitumor prodrug composites (USPIO/SQgem, USPIO/SQdox, USPIO/SQptx, and USPIO/SQcis). It should be considered that the squalenoyl prodrugs are amphiphilic molecules that may easily flip to expose the hydrophilic/hydrophobic part in response to surface medium.

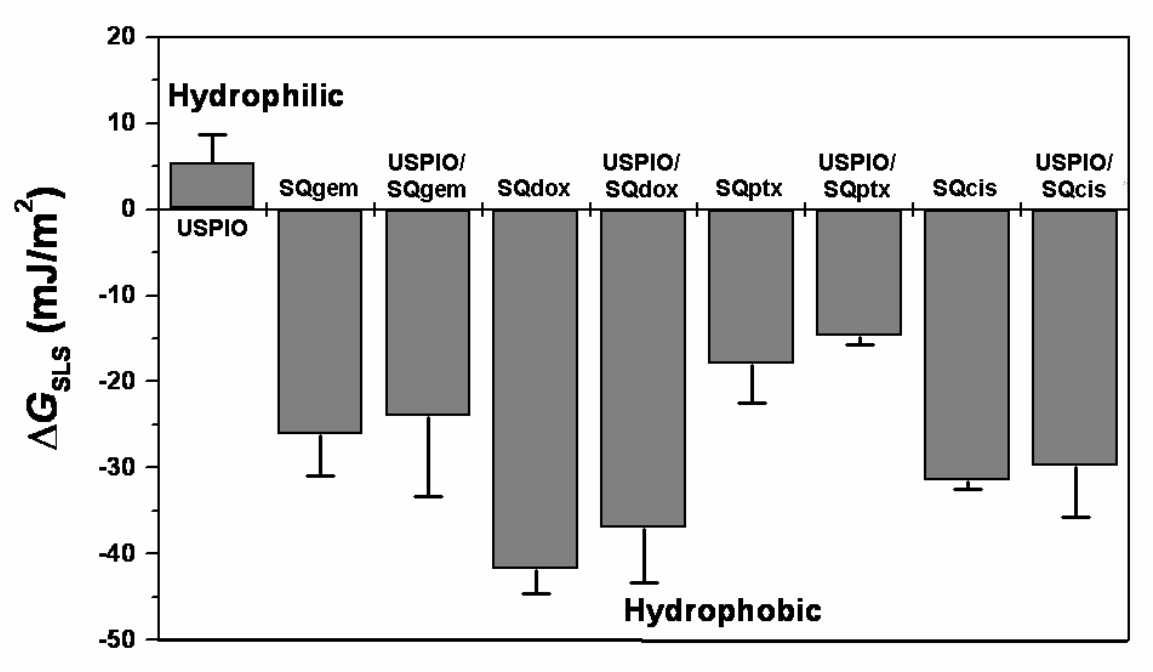

Supporting Figure 9. (a) Hysteresis cycles of nanomagnetite (■, USPIO) and nanomagnetite/squalenoyl antitumor prodrug composite NPs (USPIO/SQgem: □, USPIO/SQdox: ○, USPIO/SQptx: Δ, USPIO/SQcis: ∇) (the increasing and decreasing field ramps are almost indistinguishable); (b) visual observation of the aqueous suspension of USPIO/SQgem nanocomposites on a 1.1 T permanent magnet; (c) optical microscope picture (bar length: 10 μm) showing magnetic field induced chaining of USPIO/SQgem NPs in aqueous suspension.

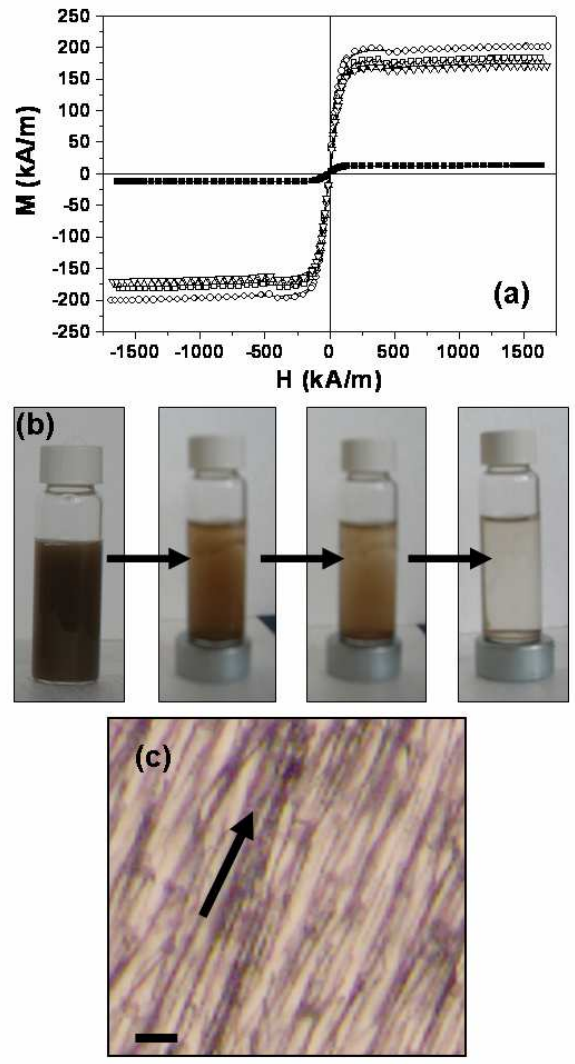

Supporting Figure 10. *In vitro* release kinetic of SQgem (■), SQdox (●), SQptx (▲), and SQcis (▼) from USPIO/SQgem, USPIO/SQdox, USPIO/SQptx, and USPIO/SQgem NPs, respectively, in PBS (pH = 7.4 ± 0.1) at 37.0 ± 0.5 ºC.

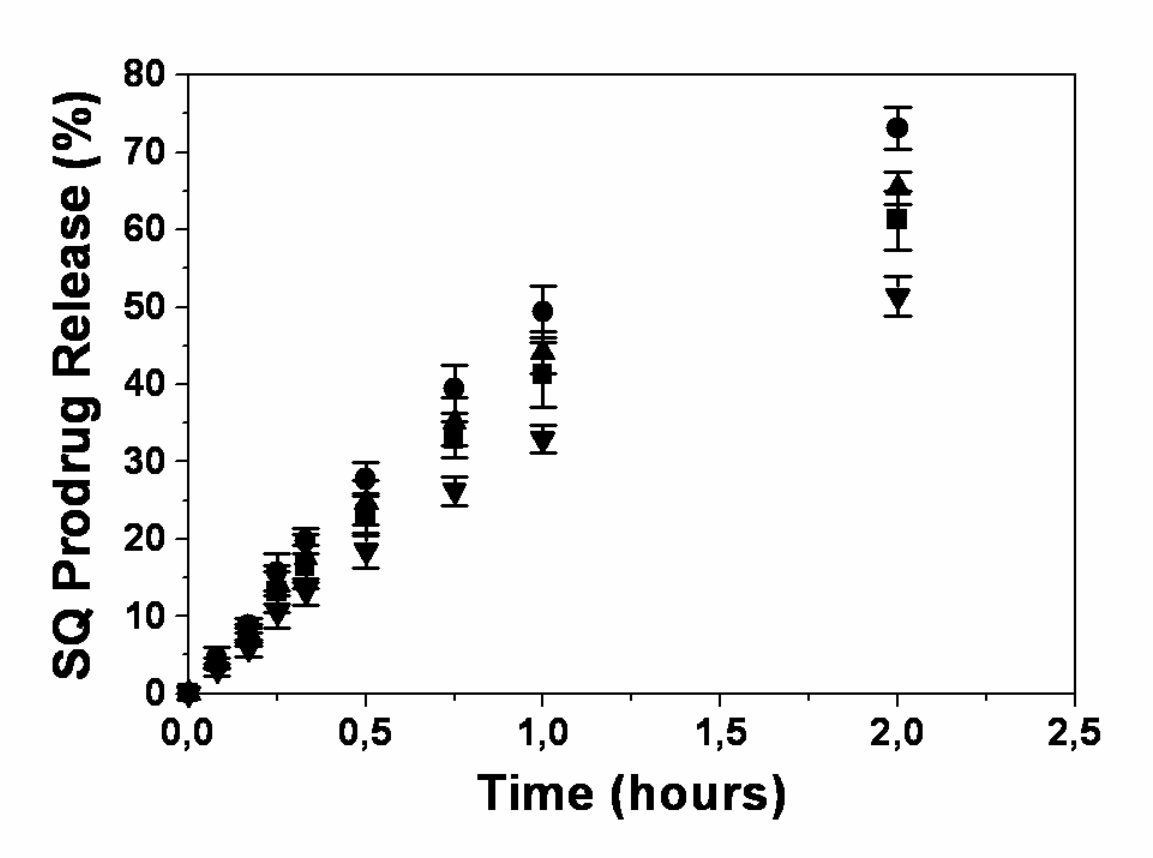

Supporting Figure 11. (A) Example of T_2-weighted image of a tumor (a) after injection of USPIO/SQgem composite NPs suspension (5 mg/Kg equivalent of gemcitabine), and (b) the corresponding T_2 map. **(B)** Example of data analysis: (a) tumor tissue before injection of USPIO/SQgem composites (5 mg/Kg equivalent of gemcitabine) and histogram, determination of the threshold ($p < 0.05$); (b) tumor tissue after injection and histogram; (c) same slice after segmentation, determination of hypo-intensity area ($T_2 < 36$ ms); and, (d) determination of the area in which $T_2 < 20$ ms.

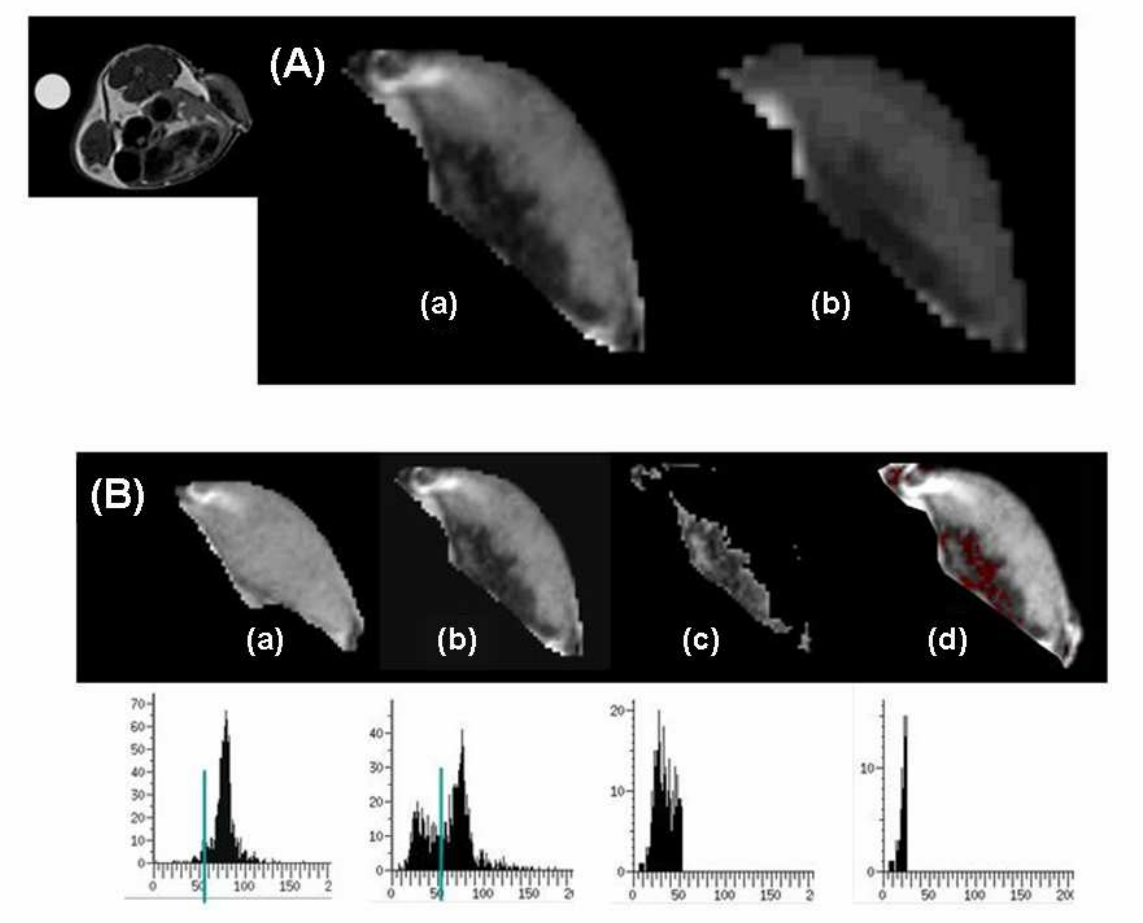

Supporting Figure 12. Immunochemical evaluation of tumors obtained from mice untreated or treated with SQgem NPs (5 mg/Kg equivalent of gemcitabine), USPIO/SQgem composites (no extracorporeal magnetic field, no-MF) (5 mg/Kg equivalent of gemcitabine) or USPIO/SQgem composites (with 1.1 T extracorporeal magnetic field for 2 h after injection, MF) (5 mg/Kg equivalent of gemcitabine). The tumors were paraffin embedded and then processed for cell proliferation test by staining the Ki-67 antigen. Tumor sections were also treated either with first antibody alone or with second antibody alone (as false controls) to determine the non-specific binding of the antibodies. The cells stained brown are Ki-67 positive cells (indicated by arrows in the images). Noteworthy, the tumor sections of mice treated with magnetically-guided USPIO/SQgem NPs showed considerably lower population of proliferating cells, comparatively to tumor sections of mice injected with other treatments.

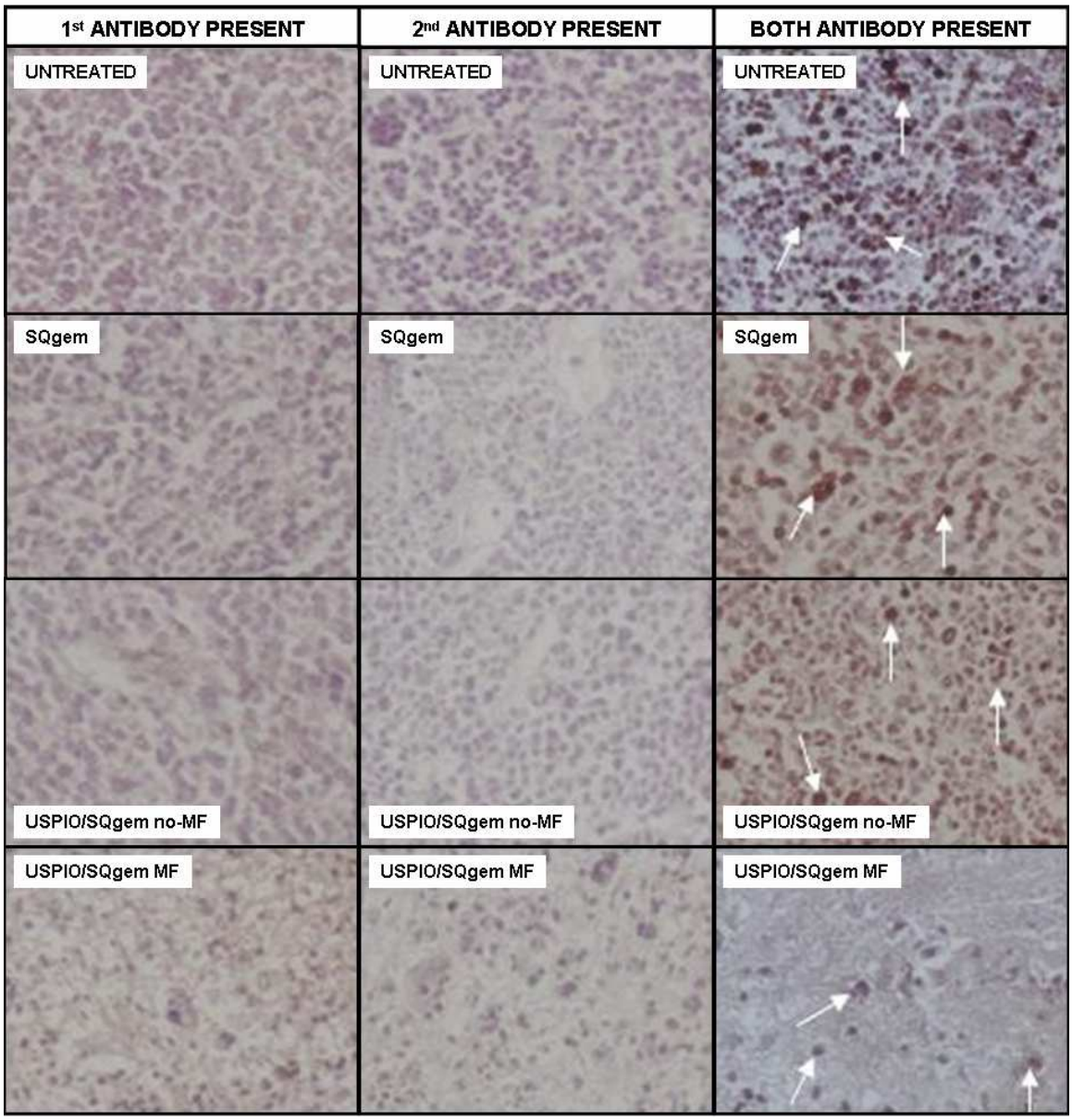
1st ANTIBODY PRESENT
2nd ANTIBODY PRESENT
BOTH ANTIBODY PRESENT
UNTREATED
UNTREATED
UNTREATED
SQgem
SQgem
SQgem
USPIO/SQgem no-MF
USPIO/SQgem no-MF
USPIO/SQgem no-MF
USPIO/SQgem MF
USPIO/SQgem MF
USPIO/SQgem MF

Supporting Figure 13. Prussian blue staining test of tumors obtained from mice untreated (negative control) or treated with USPIO/SQgem composites (no extracorporeal magnetic field, no-MF) (5 mg/Kg equivalent of gemcitabine), and USPIO/SQgem composites (with 1.1 T extracorporeal magnetic field for 2 h after injection, MF) (5 mg/Kg equivalent of gemcitabine). In case of positive control for iron, the tumor section of untreated mice was incubated with an USPIO aqueous suspension (0.15 %, w/v) for 1 min, and then washed with distilled water and treated for Prussian blue staining. The images confirmed a considerably higher accumulation of iron (especially in the tumor periphery) in the tumor tissue of magnetically-guided USPIO/SQgem NPs, as compared with USPIO/SQgem NPs non-exposed to an extracorporeal magnetic field.

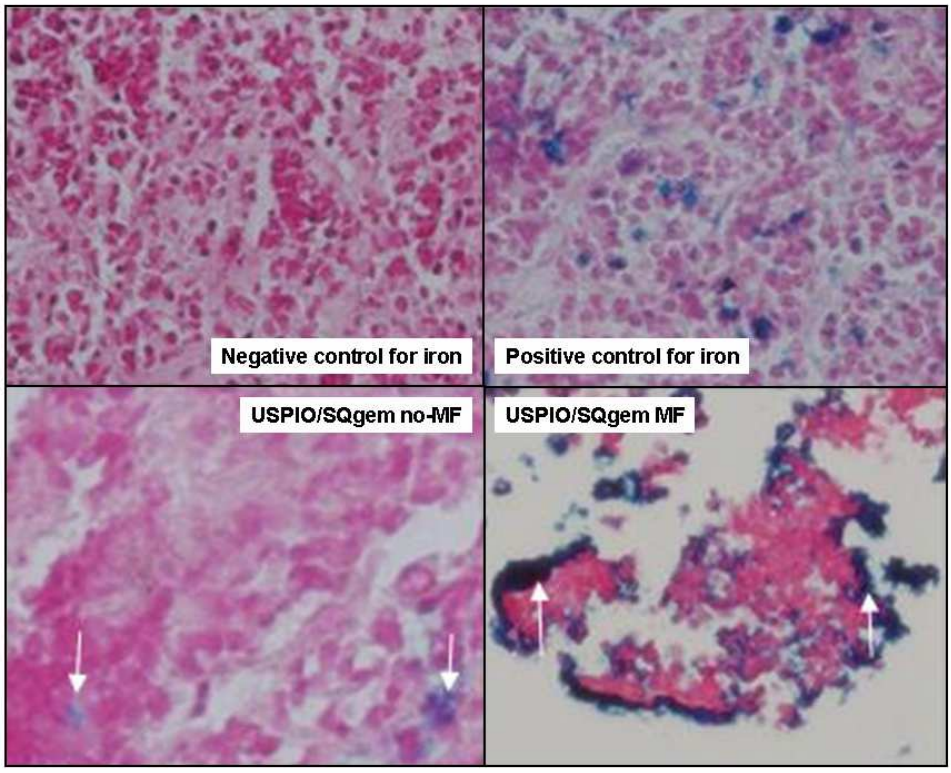

Supporting Figure 14. Small-angle X-ray scattering (SAXS) pattern of SQgem/$SQGd^{3+}$ nanocomposites in excess water. The SAXS pattern is shown on linear scale.

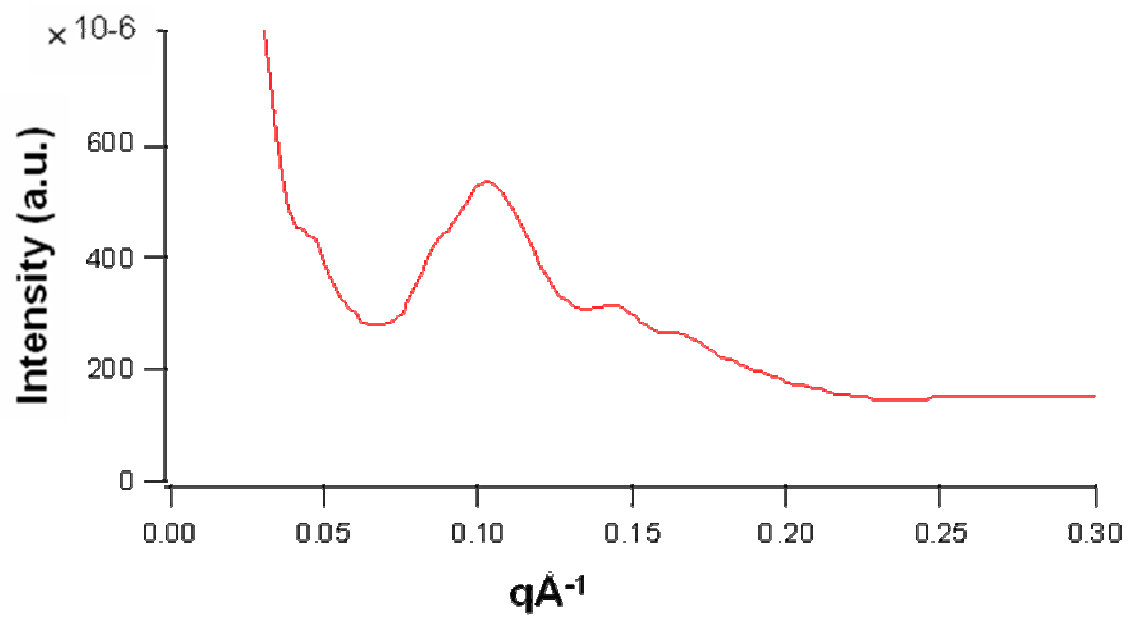

Supporting Figure 15. ^{1}H-NMRD relaxivity profile of $SQGd^{3+}$ complex in water at 310 ºK. The line corresponds to the theoretical fitting of the data points.

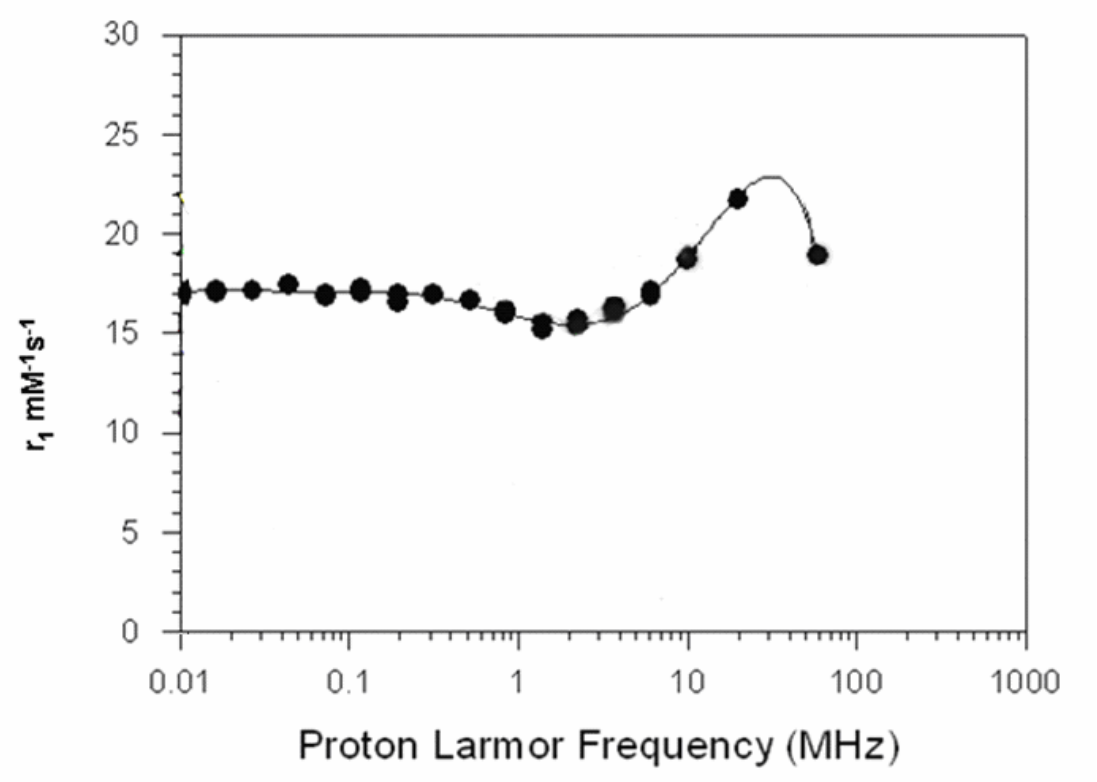

SUPPORTING TABLES

Supporting Table 1. Zeta potential (ζ), average diameter and polydispersity index, and r_1 relaxivity (measured at 20 MHz, and 37.0 ± 0.5 °C) of SQgem, $SQGd^{3+}$, and SQgem/$SQGd^{3+}$ nanoparticles (mean values ± standard deviation, n = 3).

Material	**ζ (mV)**	**Average diameter (nm)**	**Polydispersity index**	**r_1 ($mM^{-1}{\cdot}s^{-1}$)**
SQgem	-23 ± 1	120 ± 30	0.11 ± 0.04	-
$SQGd^{3+}$	-29 ± 1	7 ± 3	0.23 ± 0.05	22.1 ± 0.1
SQgem/$SQGd^{3+}$	-26 ± 1	140 ± 50	0.16 ± 0.04	20.1 ± 0.3